SAPIENZA
UNIVERSITÀ DI ROMA

FACOLTÀ DI FARMACIA E MEDICINA

PhD Course in Pharmaceutical Sciences, cycle XXVIII

PhD Student: **Adele Pirolli**

Tutor: **Prof. Rino Ragno**

INTRODUCTION

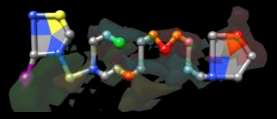

Ph.D. ACTIVITIES

TOOLS

- **DOCKING**
- **QSAR**
- **3-DQSAR**
- **COMBINE**

DESCRIPTORS ANALYSIS

FRAGMENT BASED

Washington University in St. Louis

EPIGENETICS

LSD1

- **-EXTENSIVE QSAR**
- **DESIGN NEW REVERSIBLE INHIBITORS**

HDAC

- **-COMBINE -3-DQSAR**
- **DESIGN OF SELECTIVE COMPOUNDS**

SIRT2

- **DOCKING**
- **ANALYSIS BINDING MODE AGK_2**

KDM4A

- **-DOCKING -3-DQSAR**
- **DESIGN NEW INHIBITORS**

INTRODUCTION

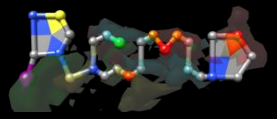

Ph.D. ACTIVITIES

TOOLS

- DOCKING
- QSAR
- 3-DQSAR
- COMBINE

DESCRIPTORS ANALYSIS

FRAGMENT BASED

NATURAL PRODUCTS

MENTA

- ESSENTIAL OIL EXTRACTION
- OPTIMAL TIME EXTRACTION STUDY

TEOMS

- PLS
- ANALYSIS COMPONENTS %

PSA

- ESSENTIAL OIL EXTRACTION
- ANTIBACTERIAL ACTIVITY OF ESSENTIAL OIL

INTRODUCTION

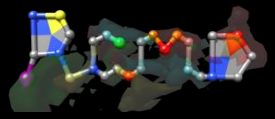

SOLUBILITY STUDY

DOCKING

QSAR
AB-INITIO

COX2

FAAH

CYP451

APPLICATIONS

ARSA

MMP

TACE

TB

UNIVERSITÉ DE LORRAINE

INNOCENTIVE

-EXTENSIVE DOCKING
-EXTENSIVE QSAR
-EXTENSIVE 3-DQSAR

VS DOCKING AND
QSAR BASED

SCREENING NIH
DATABASE
(2 HITS)

Colosseum Combinatorial Chemistry Centre for Technology

DESIGN NEW INHIBITORS

FATTY ACID AMIDE HYDROLASE (FAAH)

Endogenous ligands of cannabinoid receptors (endocannabinoids) are involved as lipid messengers in a wide array of physiological and pathological conditions, and the regulation of their levels appear to be of remarkable therapeutic interest in a variety of human disorder, including appetite, pain-sensation, mood and memory.

Twelve out of 14 experimental inhibitors were covalently bound to the catalytic Ser241. A covalent docking protocol was performed with Autodock Vina. The inhibitors were modeled and bound to Ser241 in their transition state conformation.

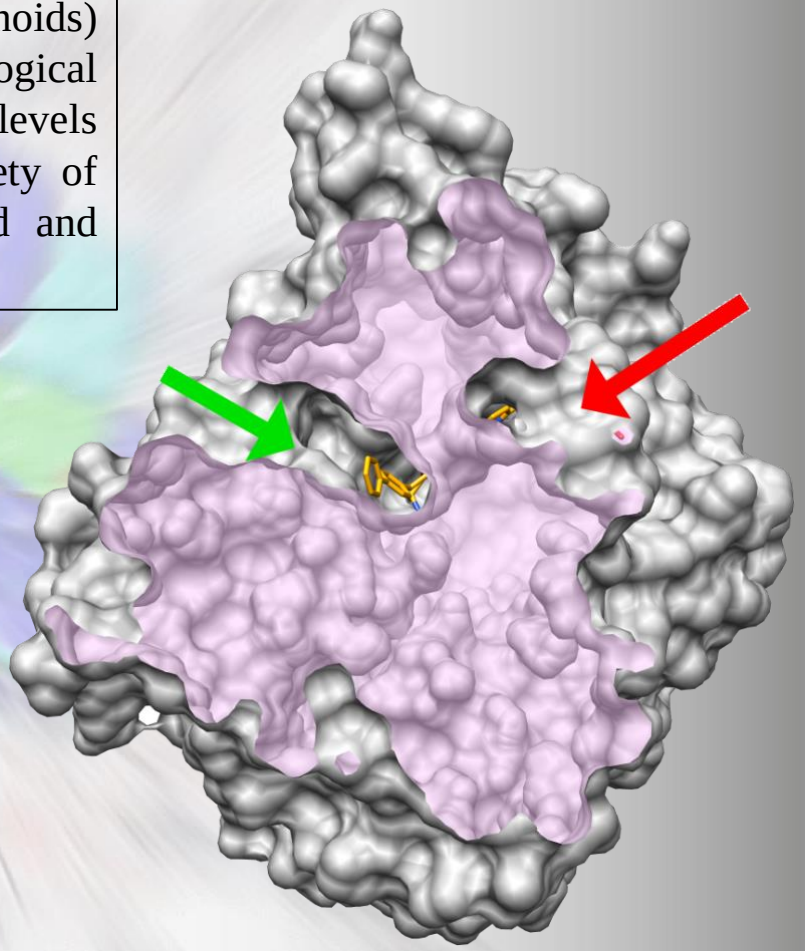

European Journal of Medicinal Chemistry
Volume 63, May 2013, Pages 118–132

Original article

Biaryl tetrazolyl ureas as inhibitors of endocannabinoid metabolism: Modulation at the *N*-portion and distal phenyl ring

Giorgio Ortar[a], Enrico Morera[a], Luciano De Petrocellis[b], Alessia Ligresti[c], Aniello Schiano Moriello[b], Ludovica Morera[a], Marianna Nalli[a], Rino Ragno[a, d], Adele Pirolli[a, d], Vincenzo Di Marzo[c]

FATTY ACID AMIDE HYDROLASE (FAAH)

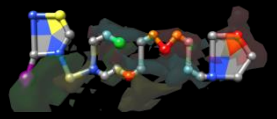

DOCKING PROCEDURE

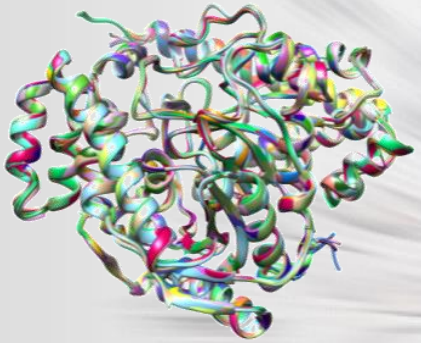

PDB

MINIMIZATION

GROMACS

DOCKING ASSESSMENT

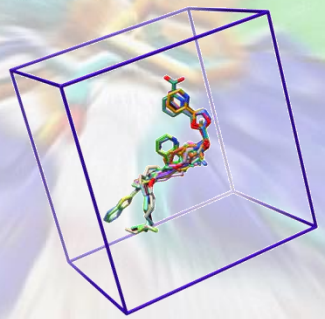

DOCKING

COVALENT DOCKING

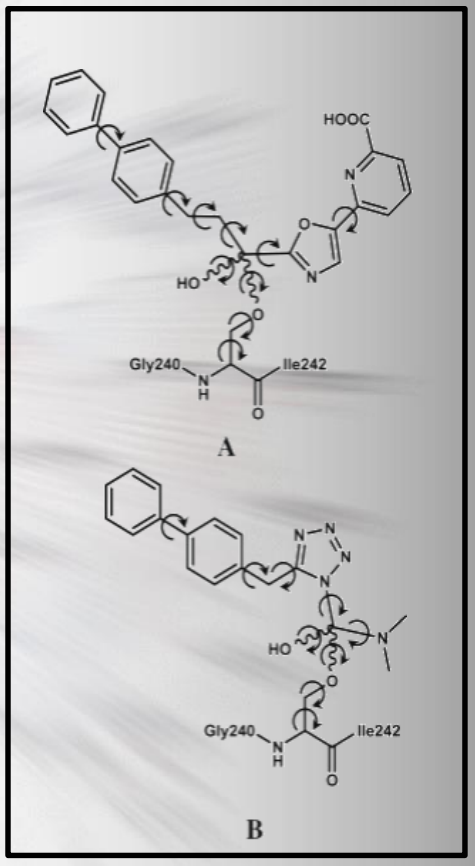

DOCKING RESULTS

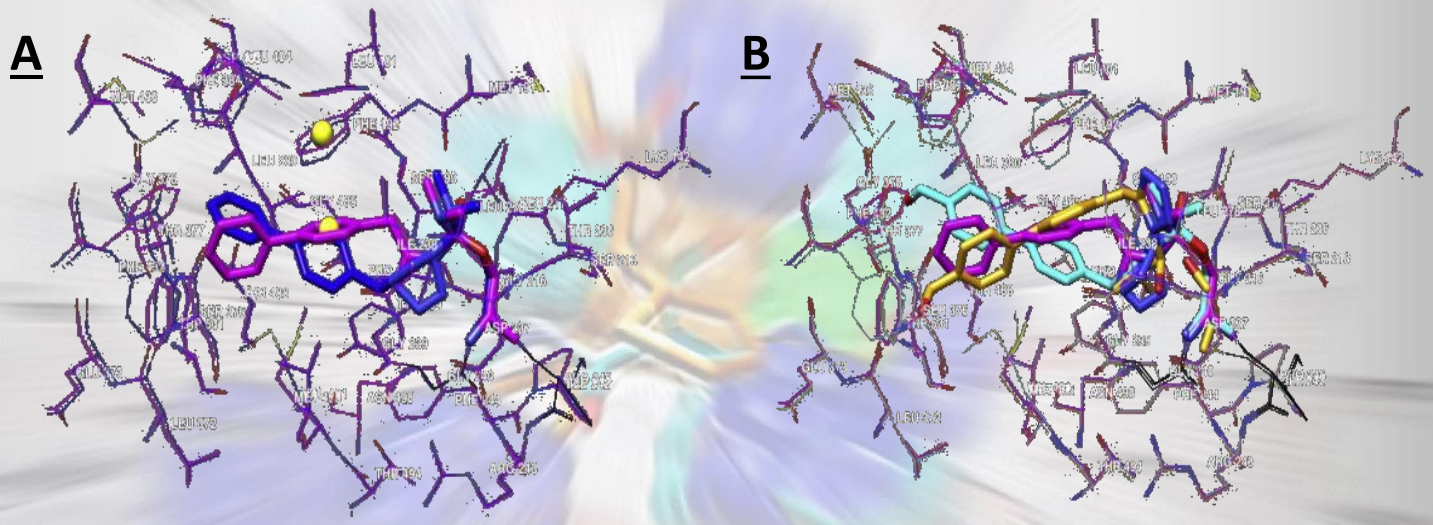

A) Binding modes of **1** (magenta) and **2** (blue) regioisomers. In yellow are highlighted the phenyl rings centroids that account for the π-π interaction between Phe192 and the 1 proximal phenyl ring. In wire are also reported the residues in a 5 Å distance from the covalent inhibitors.

B) Binding modes of the **14** (yellows) and **25** (cyan) regioisomers. In wire are also reported the residues in a 5 Å distance from the covalent inhibitors

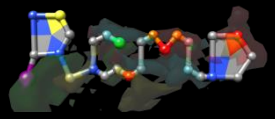

3-DQSAR PRELIMINARY RESULTS

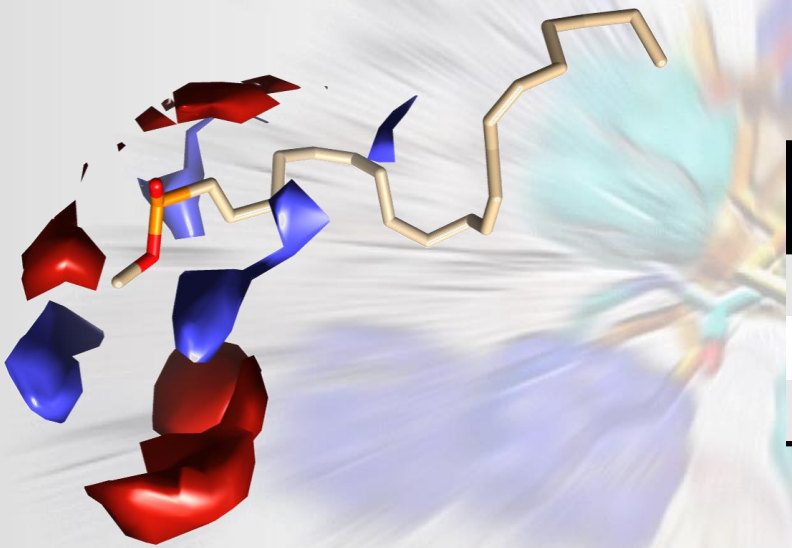

Autogrid	PC	r^2	q^2 (K5FCV)
A	2	0.86	0.52
NA	2	0.86	0.53
HD	2	0.93	0.65

PC = number of principal component analysis; r^2 = conventional correlation coefficient; q^2 = cross-validation coefficient; K5FCV = K-fold 5 random group cross validation.

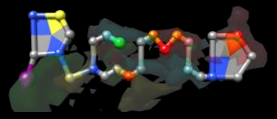

CONCLUSION

- In 23 out of 32 cases, the biphenylmethyl tetrazole moiety seem bind the hydrophobic CA channel of FAAH , with the disubstituted amino group extending into the cytosolic port.

- The investigation of the ability of tetrazoles **1-32** to act as TRPV1 and TRPA1 modulators led to identification of a potent TRPA1 activator (compound 8) which should be tested in future studies as a spinal analgesic.

CYCLOOXYGENASE (COX)

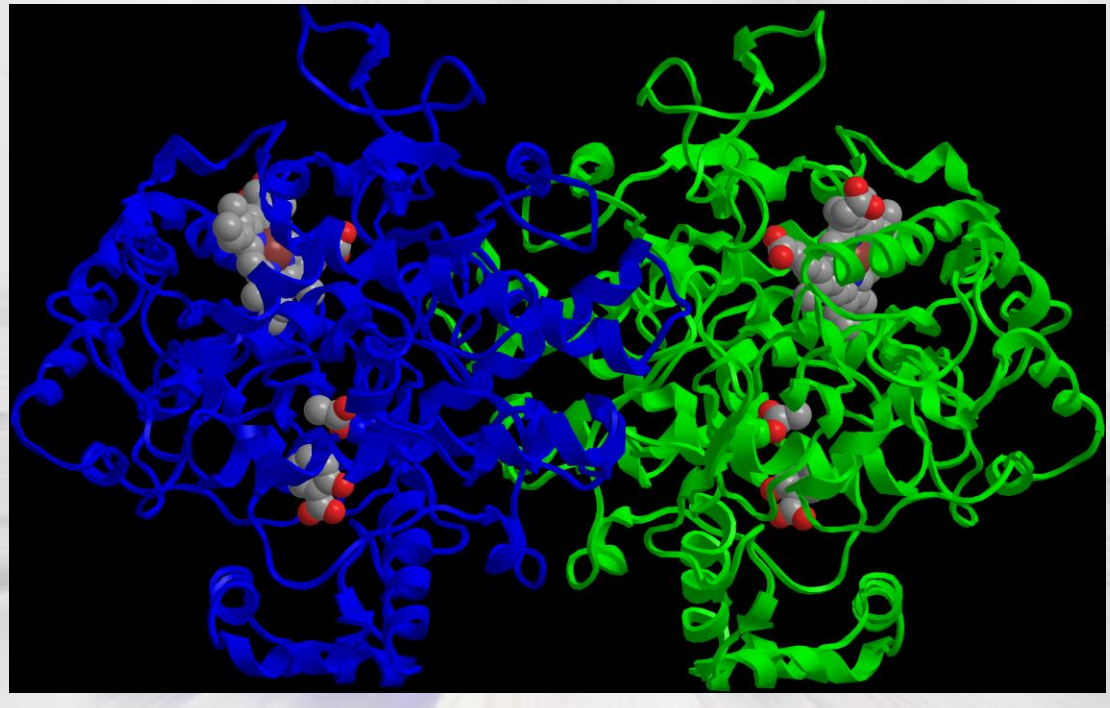

Prior any docking study, the most suitable docking program among a series of 8 program/scoring combinations function was assessed by a previously described cross-docking protocol applied on the available experimental co-crystallized complexes for either COX-1 (18 complexes) or COX-2 (14 complexes).

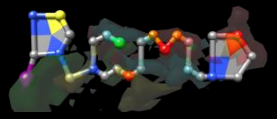

SOLUBILITY ANALYSIS

- **Eximated SOLubility (ESOL) method**

$$\mathbf{Log(S_w) = 0.16 - 0.63clogP - 0.0062MWT + 0.066\ RB - 0.74AP}$$
$$\mathbf{n=155,\ r^2=0.978,\ s=0.308}$$

- **General Solubility Equation (GSE)**

$$\mathbf{logS_w = 0.5 - 0.01(m.p.(C)-25) - logP}$$

- **ALOGPS 2.1**

CYCLOOXYGENASE (COX)

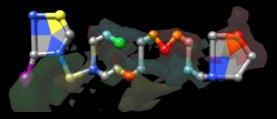

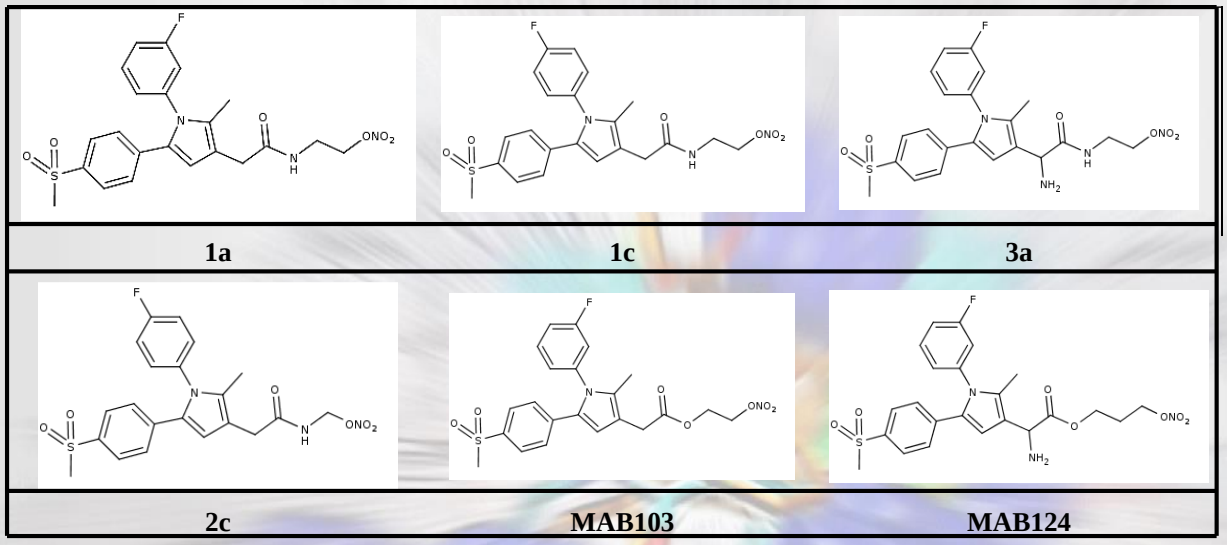

VALIDATION

	Experimental		GSE				
	SGF	PBS	MSKETCH	BABEL	VCCLAB		ALOGPS
1a	>200	80,0	-2,94	-5,28	-2,29	-6,15	-5,34
1c	>200	70,8	-2,96	-5,30	-2,30	-6,15	-5,38
3a	>200	>200	-2,27	-5,24	-2,37	-5,90	-4,70
2c	112,0	90,5	#	#	#	-6,17	-5,11
MAB103	<1,0	1,6	-3,59	-5,32	-2,46	-6,43	-5,45
MAB124	>200	80,0	-3,52	-5,59	-2,24	-6,69	-5,63

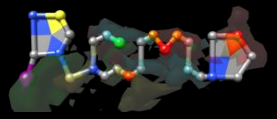

SOLUBILITY PREDICTION

			GSE				
R		**Activity (%10μM)**	**MSKETCH**	**BABEL**	**VCCLAB**	**ESOL**	**ALOGPS**
SO2CH3	1 MAB223	43	-6,35	-6,42	-2,77	-6,75	-6,33
SO2CH3	2 MAB222	65	-3,69	-6,47	-2,56	-6,75	-6,34
SO2CH3	3 MAB221	74	-3,70	-6,53	-2,51	-6,81	-6,29
SO2CH3	4 MAB220	95	-3,73	-5,54	-1,72	-6,81	-5,47
SO2NH2	5 MAB188	89	-3,69	-6,02	-2,56	-6,29	-5,36
SO2NH2	6 MAB162	82	-3,54	-5,87	-2,17	-5,94	-5,42
SO2NH2	7 MAB187	65	-3,50	-5,72	-2,02	-5,94	-4,81
SO2NH2	8 MAB161	65	-2,99	-5,21	-1,33	-5,94	-4,88
SO2NH2	9 MAB225	96	-3,79	-6,65	-2,73	-6,28	-5,99
SO2NH2	10 MAB224	62	-3,70	-6,56	-2,39	-6,28	-6,02
SO2NH2	11 MAB196	49	-3,68	-6,59	-2,44	-6,34	-6,01
SO2NH2	12 MAB194	48	-3,76	-6,67	-2,19	-6,34	-6,02

CYCLOOXYGENASE (COX)

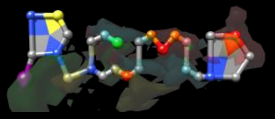

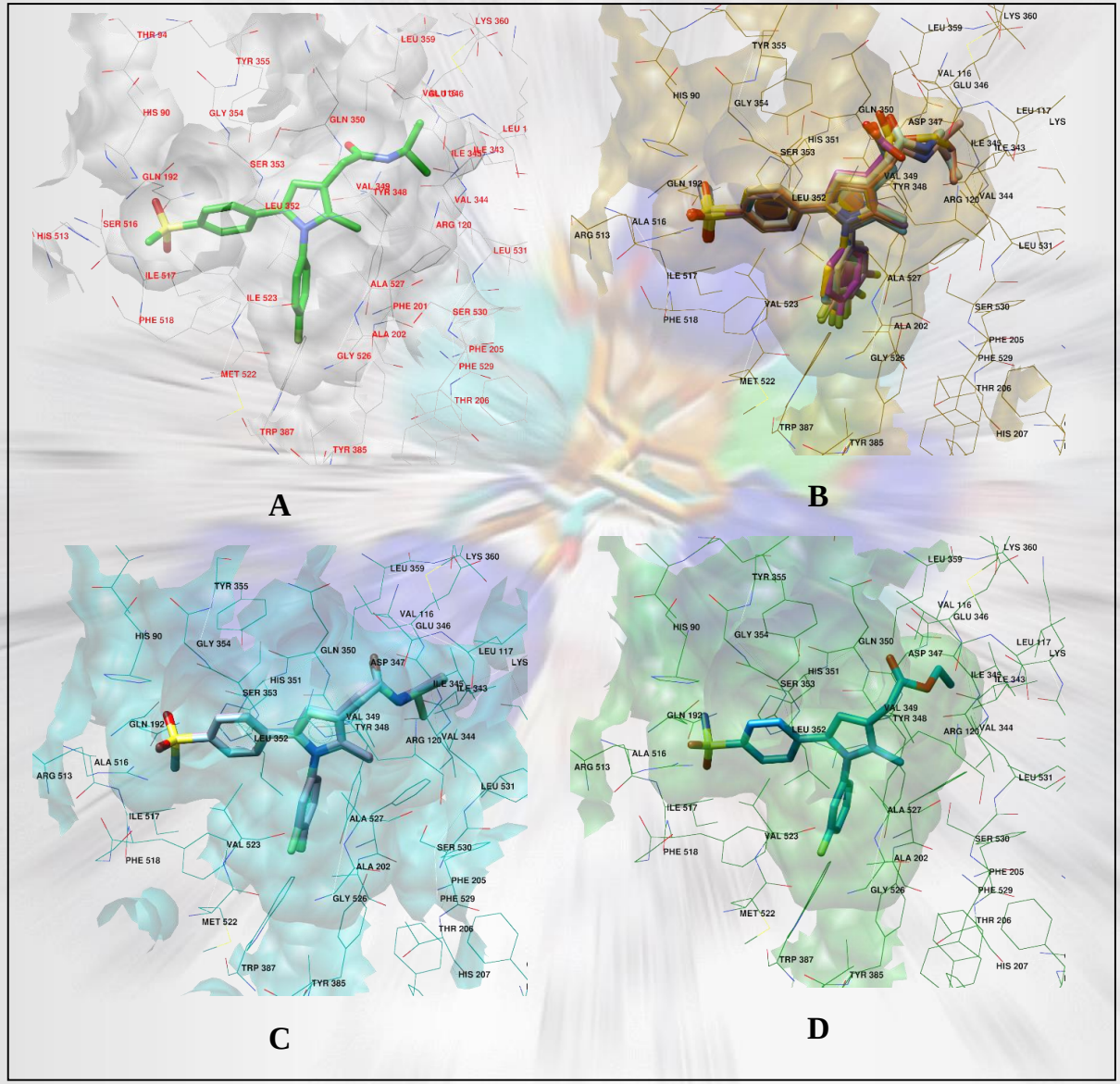

DOCKING ANALYSIS

Anti-TBC

JOURNAL OF CHEMICAL INFORMATION AND MODELING

Article

pubs.acs.org/jcim

Pharmacophore Assessment Through 3-D QSAR: Evaluation of the Predictive Ability on New Derivatives by the Application on a Series of Antitubercular Agents

Laura Friggeri,[§,†] Flavio Ballante,[*,§,‡] Rino Ragno,[*,‡] Ira Musmuca,[‡] Daniela De Vita,[†] Fabrizio Manetti,[○] Mariangela Biava,[†] Luigi Scipione,[†] Roberto Di Santo,[⊥,†] Roberta Costi,[⊥,†] Marta Feroci,[∥] and Silvano Tortorella[†]

[‡]Rome Center for Molecular Design and [⊥]Istituto Pasteur-Fondazione Cenci Bolognetti, [†]Dipartimento di Chimica e Tecnologie del Farmaco, Sapienza Università di Roma, P. le A. Moro 5, 00185 Rome, Italy

[○]Dipartimento di Biotecnologie, Chimica e Farmacia, Università degli Studi di Siena, Via Aldo Moro 2, I-53100 Siena, Italy

[∥]Dipartimento di Scienze di Base e Applicate per l'Ingegneria, Sapienza Università di Roma, Via Castro Laurenziano 7, I-00161 Rome, Italy

Supporting Information

ABSTRACT: Pharmacophoric mapping is a useful procedure to frame, especially when crystallographic receptor structures are unavailable as in ligand-based studies, the hypothetical site of interaction. In this study, 71 pyrrole derivatives active against *M. tuberculosis* were used to derive through a recent new 3-D QSAR protocol, 3-D QSAutogrid/R, several predictive 3-D QSAR models on compounds aligned by a previously reported pharmacophoric application. A final multiprobe (MP) 3-D QSAR model was then obtained configuring itself as a tool to derive pharmacophoric quantitative models. To stress the applicability of the described models, an external test set of unrelated and newly synthesized series of R-4-amino-3-isoxazolidinone derivatives found to be active at micromolar level against *M. tuberculosis* was used, and the predicted bioactivities were in good agreement with the experimental values. The 3-D QSAutogrid/R procedure proved to be able to correlate by a single multi-informative scenario the different activity molecular profiles thus confirming its usefulness in the rational drug design approach.

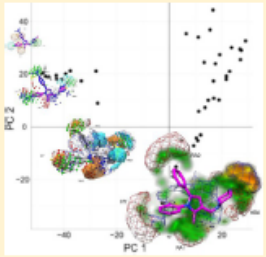

Pharmacophore assessment through 3-D QSAR: evaluation of the predictive ability on new derivatives by the application on a serie of antitubercular agents. L. Friggeri, Ballante Flavio, R. Ragno, I. Musmuca, D. De Vita, F. Manetti, M. Biava, L. Scipione, R. Di Santo, R. Costi, M. Feroci, S. Tortorella (2013). *Journal Of Chemical Information And Modeling*; p 1463–1474, ISSN: 1549-9596, doi: 10.1021/ci400132q

Anti-TBC

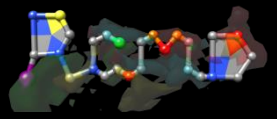

Training Set : **71 cmpds**

Activity Range (pMIC):
*(2.47 Log unit, σ=**0.71**)*

QSAR/SKLEARN LIBRARIES

12 MODELS

Loss = ls, lad, huber ← GBR

C = 10, 100, 1000 ← SVM

ET

RF

BAYES

Statistical/graphical Analyses

Prediction

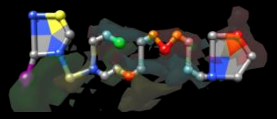

QSAR RESULTS LOO

	q2_raw	q2	r2_raw	r2	features
S.BoostingRegressor(lad)	0,82	0,84	0,98	0,97	66
S.BoostingRegressor(ls)	0,77	0,86	1,00	1,00	64
S.BoostingRegressor(huber)	0,79	0,86	1,00	0,99	62
KNeighborsRegressor	0,56	0,75	0,69	0,82	61
GradientBoostingRegressor(huber)	0,71	0,87	0,99	1,00	5
BayesianRidge	0,83	0,89	0,90	0,91	18
PLSRegression(3)	0,75	0,81	0,81	0,84	29
SVR	-0,02	0,75	0,98	0,97	39
GradientBoostingRegressor(ls)	0,69	0,88	1,00	1,00	53
RandomForestClassifier	0,64	0,76	0,99	0,95	66
ExtraTreesRegressor	0,82	0,83	1,00	1,00	66
GradientBoostingRegressor(lad)	0,78	0,86	0,98	0,97	54

Anti-TBC

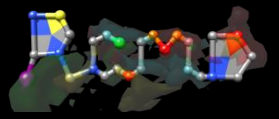

- A conjuction between the obtained 3-D QSARs and new ad-hoc QSAR models was then adopted in a Virtual Screening (VS) application in order to identify new potential antitubercular agents from the NCI Diversity Set.

- The VS:

  was applied only to compounds which have physico-chemical characteristics similar to those of the original Training Set.

  was previously validated over compounds (taken from the CHEMBL database) for which was known the antitubercular activity, in order to :

  1. select the best QSAR chemometric approach
  2. assess the Ligand-Based alignment procedure to adopt over the target database (NCI Diversity Set).

- Applying the consensous scoring 'Range Scale' procedure, were finally selected 120 compounds, for which the anti-mycobacterial activity will be determined.

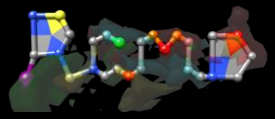

QSAR Modeling of KDM1A Inhibitors Using Machine Learning Approaches.

***Adele Pirolli**, Alexandros Patsilinakos, and Rino Ragno*

LSD1

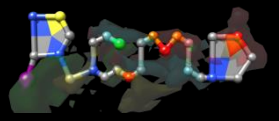

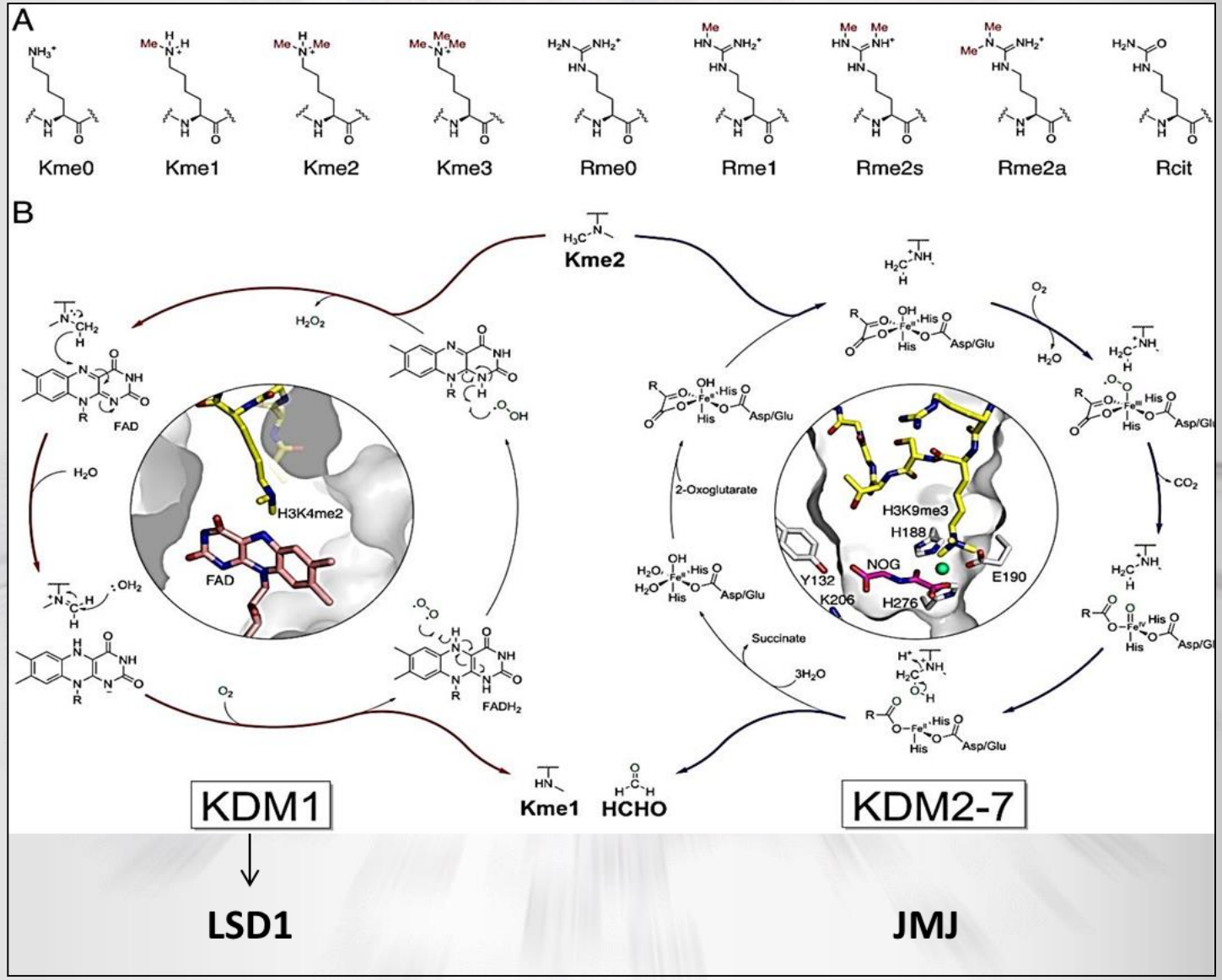
A
Kme0
Kme1
Kme2
Kme3
Rme0
Rme1
Rme2s
Rme2a
Rcit
B
Kme2
H2O2
FAD
H2O
H3K4me2
FAD
FADH2
O2
Kme1
HCHO
KDM1
LSD1
2-Oxoglutarate
Succinate
3H2O
CO2
H3K9me3
H188
NOG
Y132
K206
H276
E190
Asp/Glu
His
KDM2-7
JMJ

LSD1

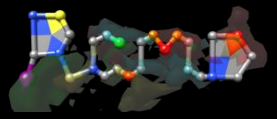

Experimantal Structure Activity Data

Test Set | Training Set

↓

Calculation of Molecular Descriptors

↓

QSAR Model Generation

Model Accepted?

↓

Prediction of Test Set Data

↓

External Validation

↓

De novo Design and/or Virtual Screening

↓

Experimental Training

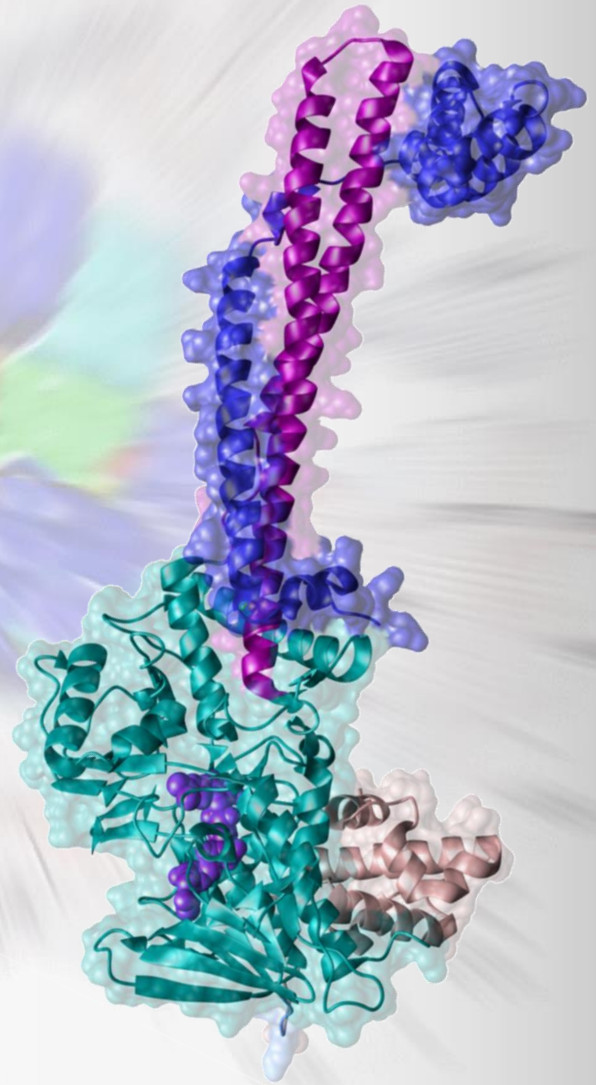

LSD1

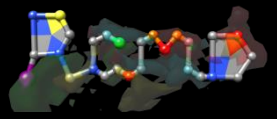

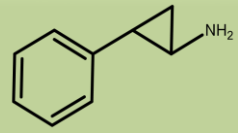

TRANILCIPROMINE

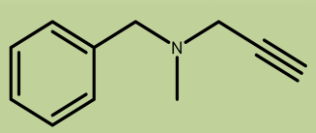

PARGILINE

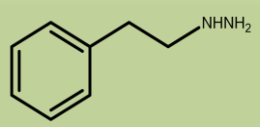

FENELZINE

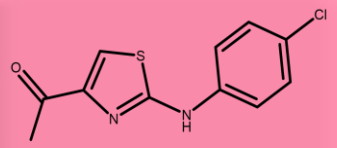

HITCHIN et al.

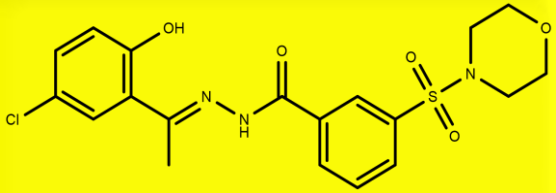

SORNA et al.

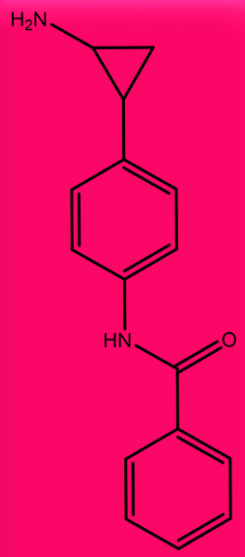

MAI et al.

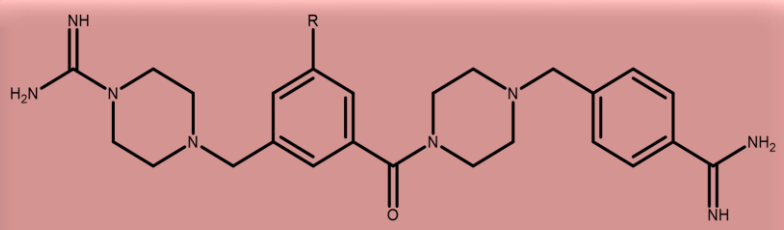

WANG et al.

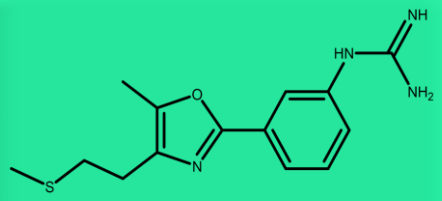

DULLA et al.

LSD1

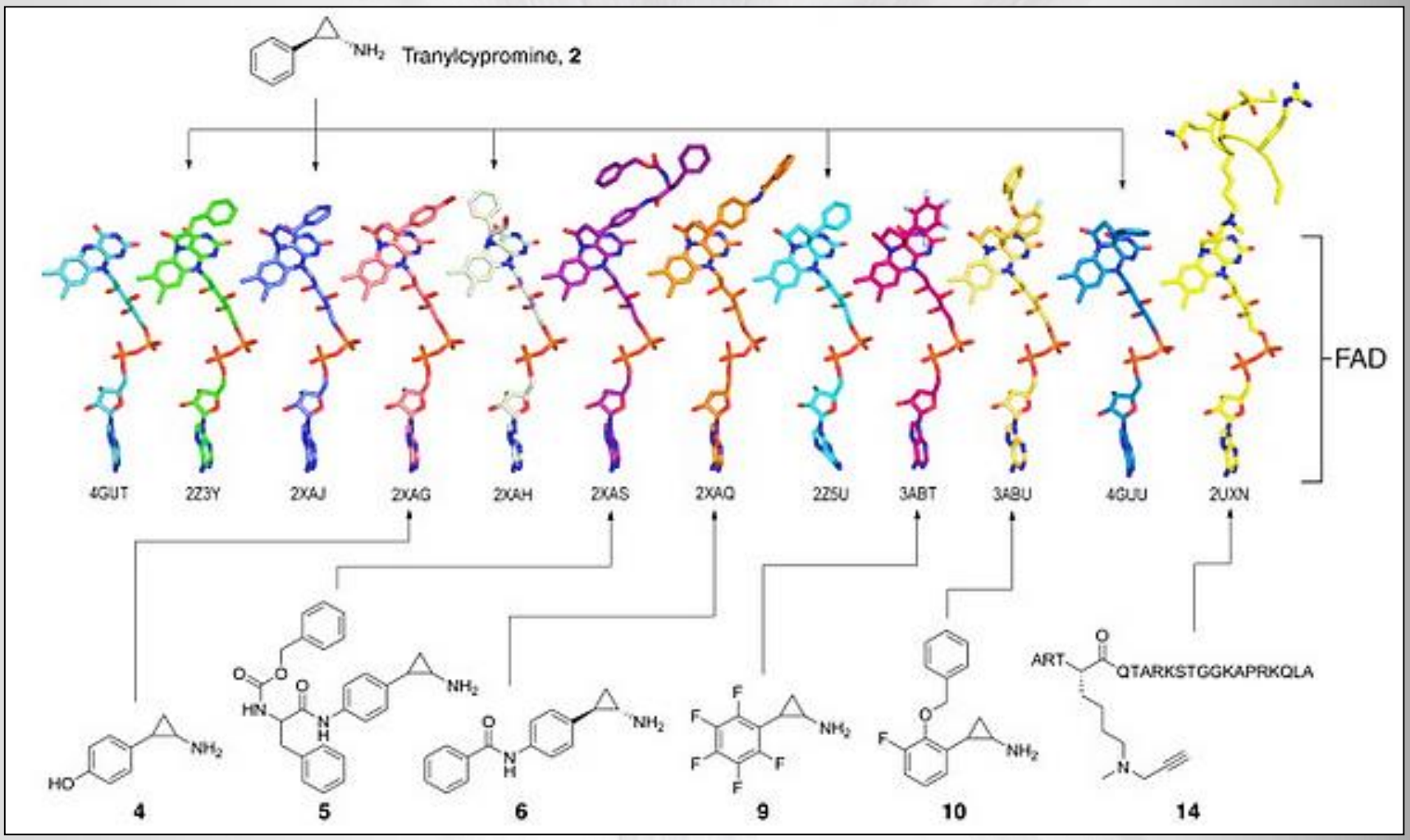
Tranylcypromine, 2
FAD
4GUT
2Z3Y
2XAJ
2XAG
2XAH
2XAS
2XAQ
2Z5U
3ABT
3ABU
4GUU
2UXN
4
5
6
9
10
14
ART
QTARKSTGGKAPRKQLA

LSD1

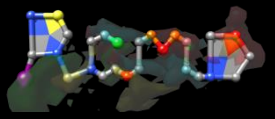

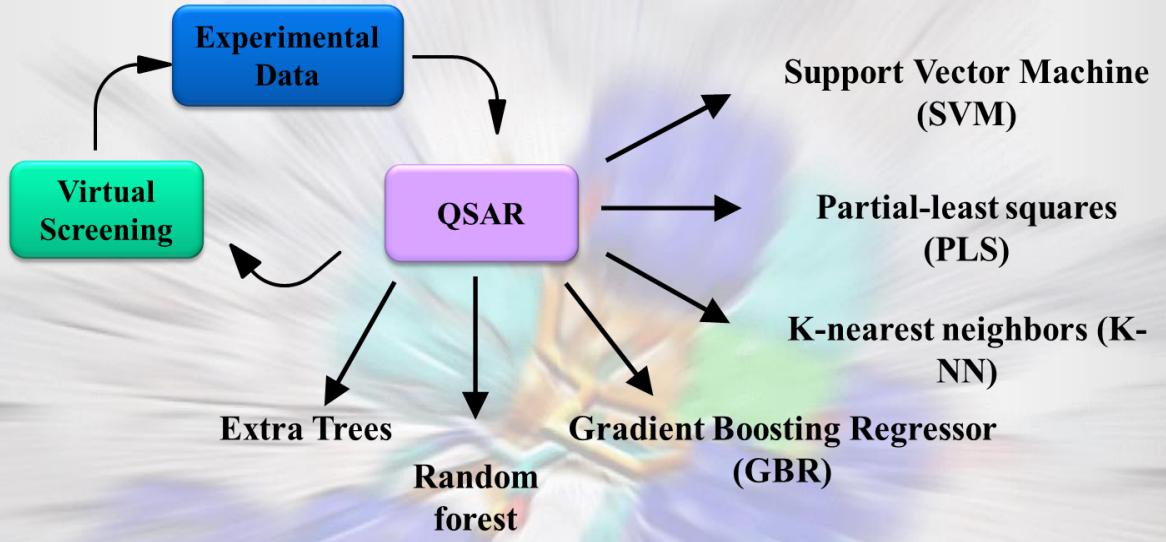

CV loo	r^2	q^2	# features
PLS Regression (3 PCs)	0.91	0.86	21
GBR (LAD)	0.99	0.88	60
GBR (HUBER)	0.99	0.87	59
GBR	0.99	0.85	62
SBR (LAD)	0.99	0.85	80
SBR (HUBER)	0.99	0.86	76
SBR	0.99	0.84	78
BAYESAN	0.99	0.99	31
SVM	0.99	0.69	9
KNN	0.84	0.76	78
RANDOM FOREST	0.99	0.79	79
EXTRA TREE	0.99	0.86	79

LSD1

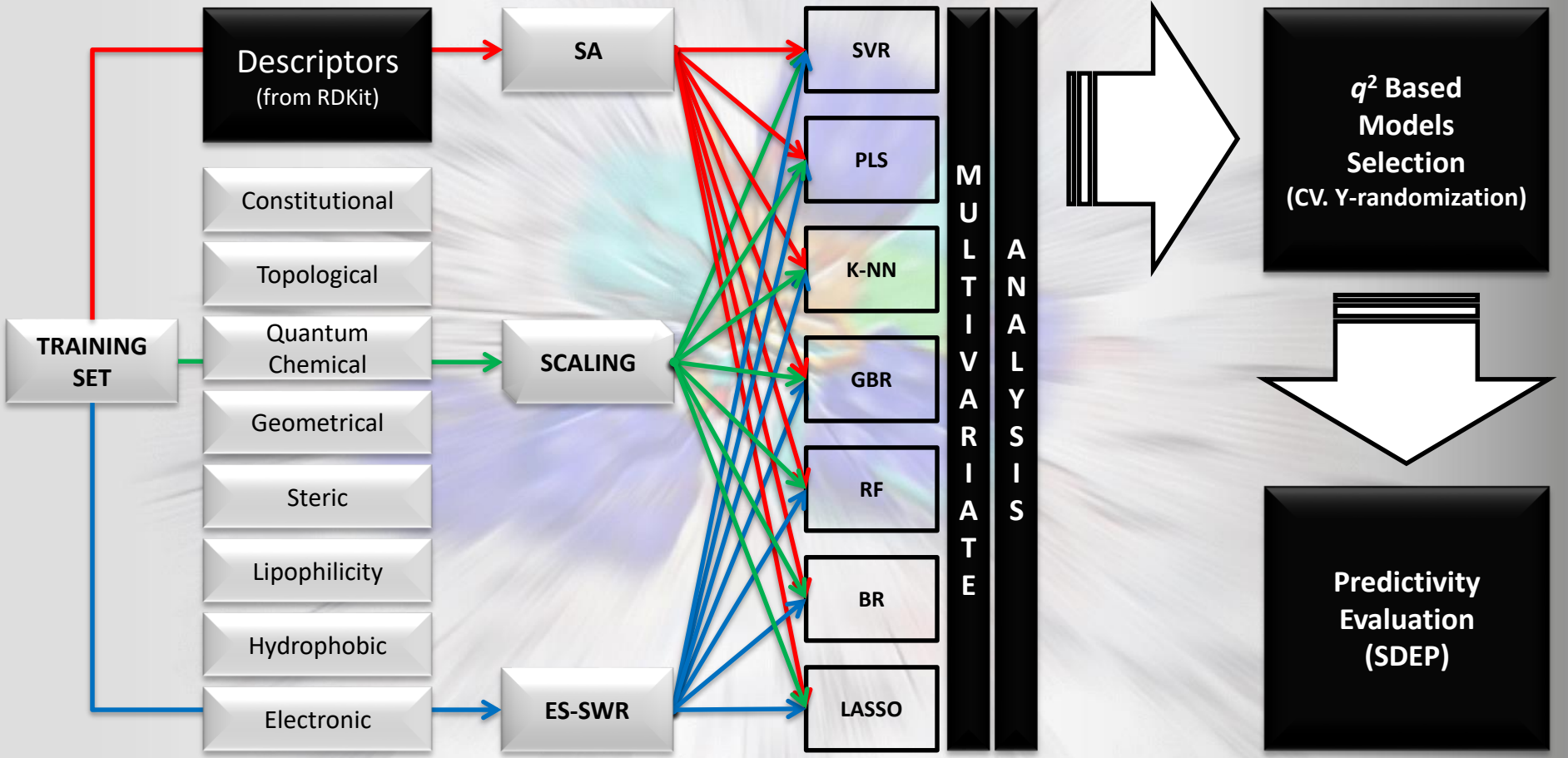
Descriptors
(from RDKit)
Constitutional
Topological
Quantum Chemical
Geometrical
Steric
Lipophilicity
Hydrophobic
Electronic
TRAINING SET
SA
SCALING
ES-SWR
SVR
PLS
K-NN
GBR
RF
BR
LASSO
MULTIVARIATE ANALYSIS
q^2 Based Models Selection
(CV. Y-randomization)
Predictivity Evaluation
(SDEP)

LSD1

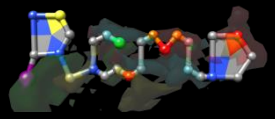

Data Set	Method	K-fold				Y-scrambling						External Validation		
		q^2	r^2	SDEP	SDEC	Average q^2	Average r^2	Average SDEP	Average SDEC	Maximum q^2	Number of positive q^2	SDEP	AAEP	r^2_{pred}
Reversible	PLS	0.73	0.90	0.92	0.44	-0.65	0.48	1.60	0.91	0.02	1	0.45	0.36	0.90
	KNN	0.89	0.95	0.80	0.35	-0.60	0.48	1.57	0.90	0.02	1	0.42	0.37	0.92
	BR	0.89	0.96	0.93	0.28	-0.08	0.06	1.30	1.22	0.16	3	1.04	0.68	0.50
	SVR	0.69	0.99	0.69	0.11	-0.45	0.78	1.50	0.57	0.14	2	0.78	0.63	0.70
	GBR	0.74	0.98	0.79	0.14	-0.64	0.96	1.59	0.23	-0.03	0	0.37	0.35	0.94
	RF	0.79	0.98	0.92	0.48	-0.34	0.77	1.44	0.60	0.16	8	0.63	0.52	0.90
Covalent	PLS	0.82	0.88	0.75	0.46	-0.78	0.24	1.50	0.99	0.04	1	0.62	0.44	0.72
	KNN	0.46	0.84	0.83	0.46	-0.53	0.50	1.40	0.81	0.02	0	0.87	0.53	0.49
	BR	0.83	0.92	0.71	0.45	-0.07	0.06	1.17	0.11	0.11	4	1.16	0.87	0.23
	SVR	0.79	0.99	0.78	0.11	-0.95	0.90	1.57	0.35	-0.11	0	1.17	0.93	0.19
	GBR	0.67	0.99	0.82	0.05	-0.60	0.98	1.43	0.16	0.1	3	0.77	0.45	0.58
	RF	0.56	0.88	0.91	0.37	-0.35	0.78	1.31	0.54	0.37	3	0.53	0.46	0.79

LSD1

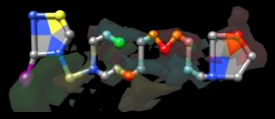

Unified Data Set													
Method	K-fold				Y-scrambling						External Validation		
	q^2	r^2	SDEP	SDEC	Average q^2	Average r^2	Average SDEP	Average SDEC	Maximum q^2	Number of positive q^2	SDEP	AAEP	r^2_{pred}
PLS	0.69	0.79	0.82	0.61	-0.36	0.29	1.42	1.03	0.01	1	0.89	0.67	0.69
KNN	0.69	0.82	0.88	0.56	-0.36	0.30	1.43	1.01	-0.10	0	0.97	0.66	0.42
BR	0.75	0.85	0.99	0.69	-0.03	0.04	1.24	1.20	0.07	5	1.58	0.85	0.17
SVR	0.77	0.99	0.74	0.11	-0.92	0.90	1.69	0.38	-0.11	0	1.06	0.95	0.34
GBR	0.77	0.99	0.77	0.10	-0.43	1.46	0.93	0.31	-0.06	0	0.74	0.59	0.65
RF	0.63	0.92	0.84	0.39	-0.04	0.03	1.29	1.21	0.02	4	0.69	0.52	0.73

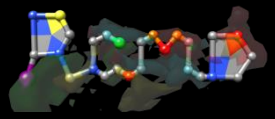

Discovery of the first Arylsulfatase A Inhibitor

Adele Pirolli, Sergio Valente, Fabio Altieri, Antonello Mai, Rino Ragno, and Gilbert Kirsch

ARYL SULFATASE A (ARSA)

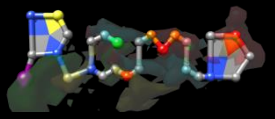

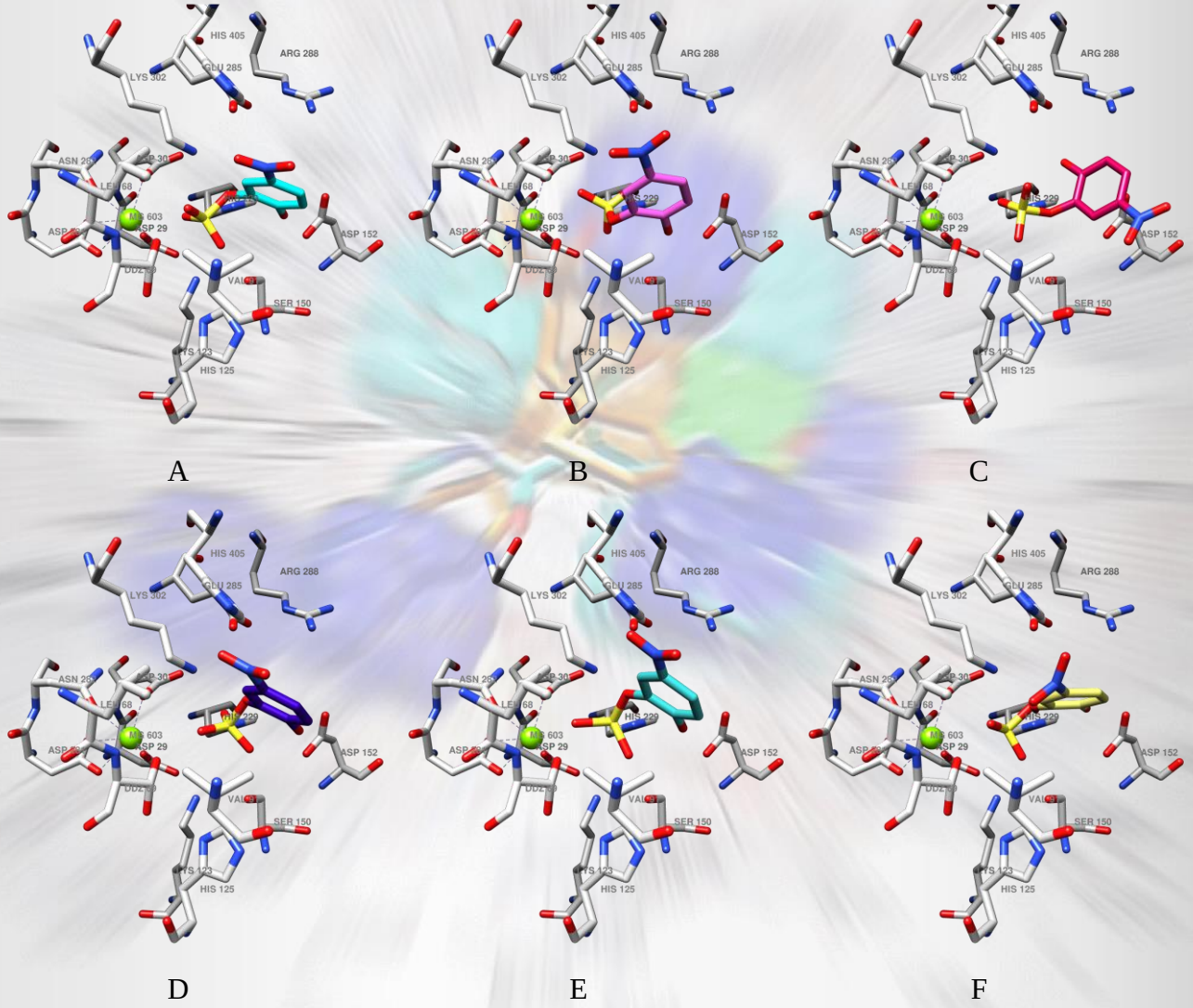

ARYL SULFATASE A (ARSA)

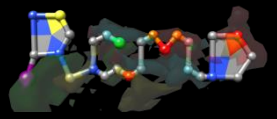

Re-docking assessment using 1e2s data. Values are the RMSD respect the experimental p-nitrocatechol sulfate conformation.		
Docking Program	**ECRD**	**RCRD**
Autodock	1.276	1.139
Autodock Vina	0.595	0.605
Plants	1.140	1.095
Surflex	0.862	1.303
Paradocks	0.952	0.818

Cross-docking assessment using other six ARSA crystals. Values are the RMSD respect the experimental p-nitrocatechol sulfate conformation.						
Docking Program	**ARSA crystals PDB entry codes**					
	1AUK	1E1Z	1E33	1E3C	1N2K	1N2L
Autodock	1.071	1.289	0.996	0.823	2.380	3.005
Autodock Vina	0.818	3.019	2.632	2.701	5.725	5.193
Plants	0.867	1.132	1.809	1.172	7.956	7.024
Surflex	2.927	2.909	1.903	2.640	4.431	5.075
Paradocks	1.035	0.763	0.621	1.314	3.095	2.475

ARYL SULFATASE A (ARSA)

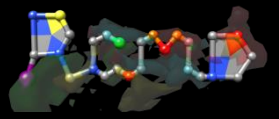

SYNTHESIS

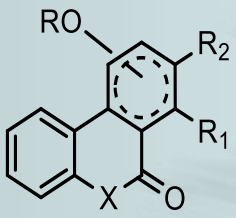

X= O, NH

A

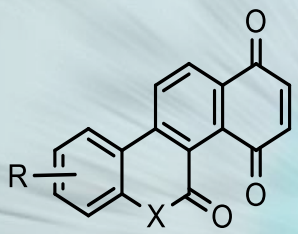

X= O, NH

B

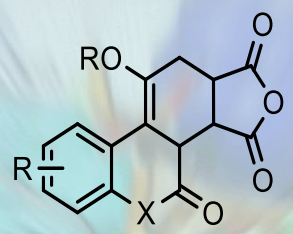

X= O, NH

C

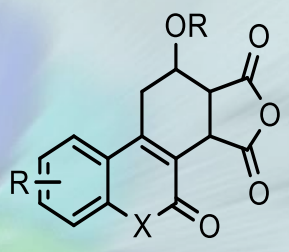

X= O, NH

D

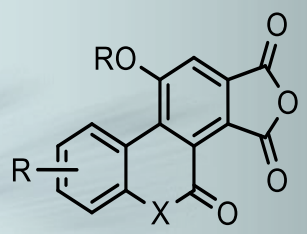

X= O, NH, S, Se

E

Among the five series, A and B were designed as potential non-covalent sulfatase inhibitors, while docking of the anhydrides C, D and E revealed that could act as irreversible inhibitors. In figure 3 is possible to view the putative binding modes of two derivatives of series E in which the anhydride moieties are at about 3.5 Å away from the FGL69 sulfatase active residues suggesting that the anhydride can be attacked by the hydrated formyl hydroxy group.

ARYL SULFATASE A (ARSA)

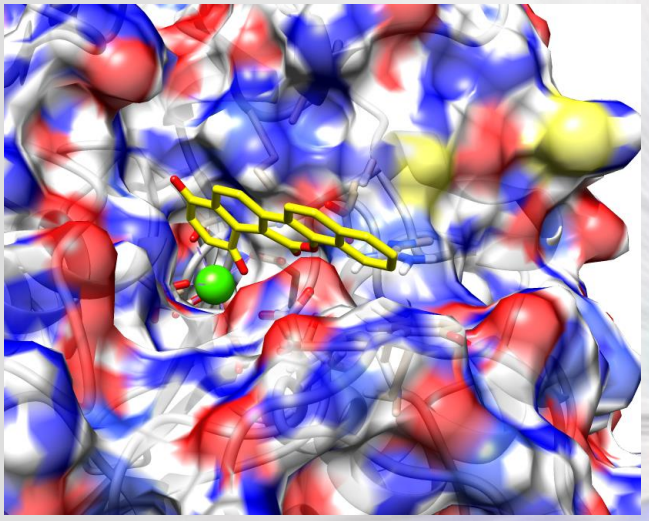

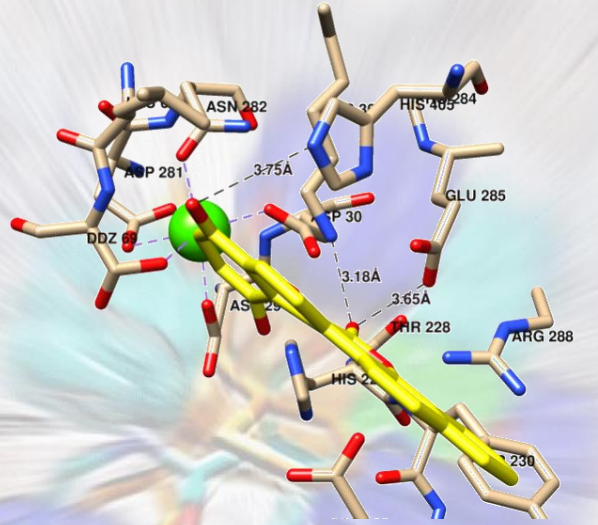

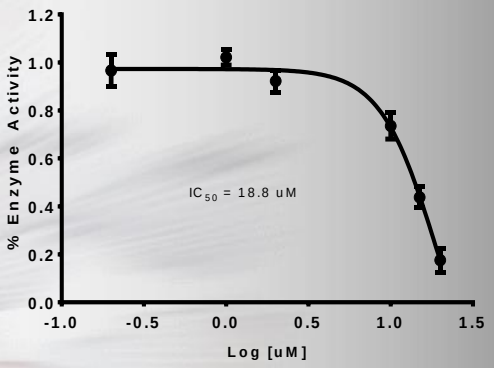

IC_{50} (µM) values percentage of living cells determinated at 3 concentrations.				
Carcinoma cell lines	IC_{50}	% cells remaining alive		
		1	10	100
A549	70	74	67	41
MCF7	7	58	40	21
PC3	75	83	77	35
Non carcinoma cell lines				
U373n glioma	55	62	61	26
Hs683 glioma	4	55	48	37
SKMEL28 melanoma	>100	77	57	48

CANDIDA

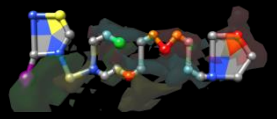

Design of a new scaffold of 1,3-thiazolidin-4-one derivatives as promising antifungal agents endowed with low cytotoxicity.

GENERAL PROCEDURE 1

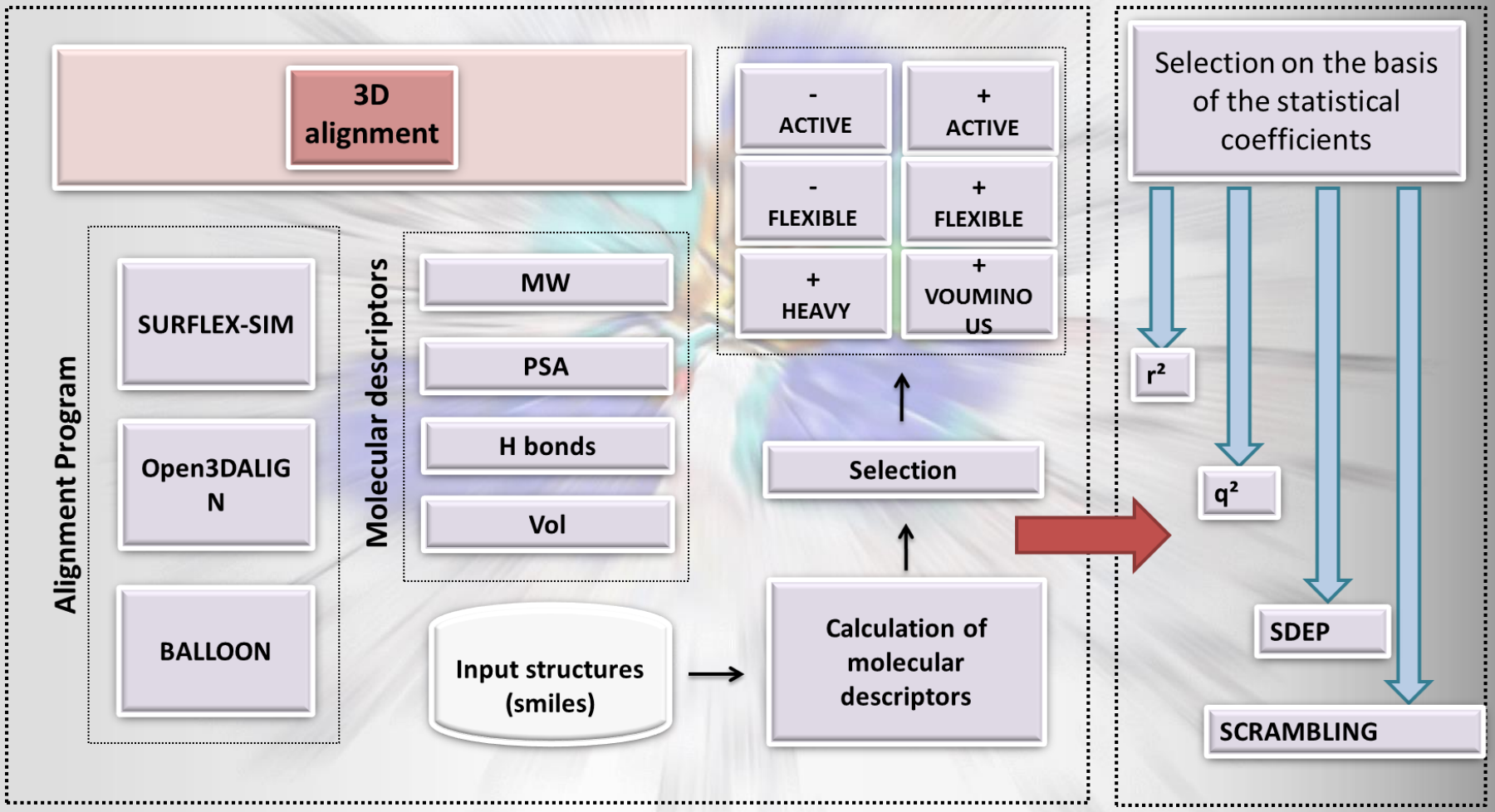

GENERAL PROCEDURE 2

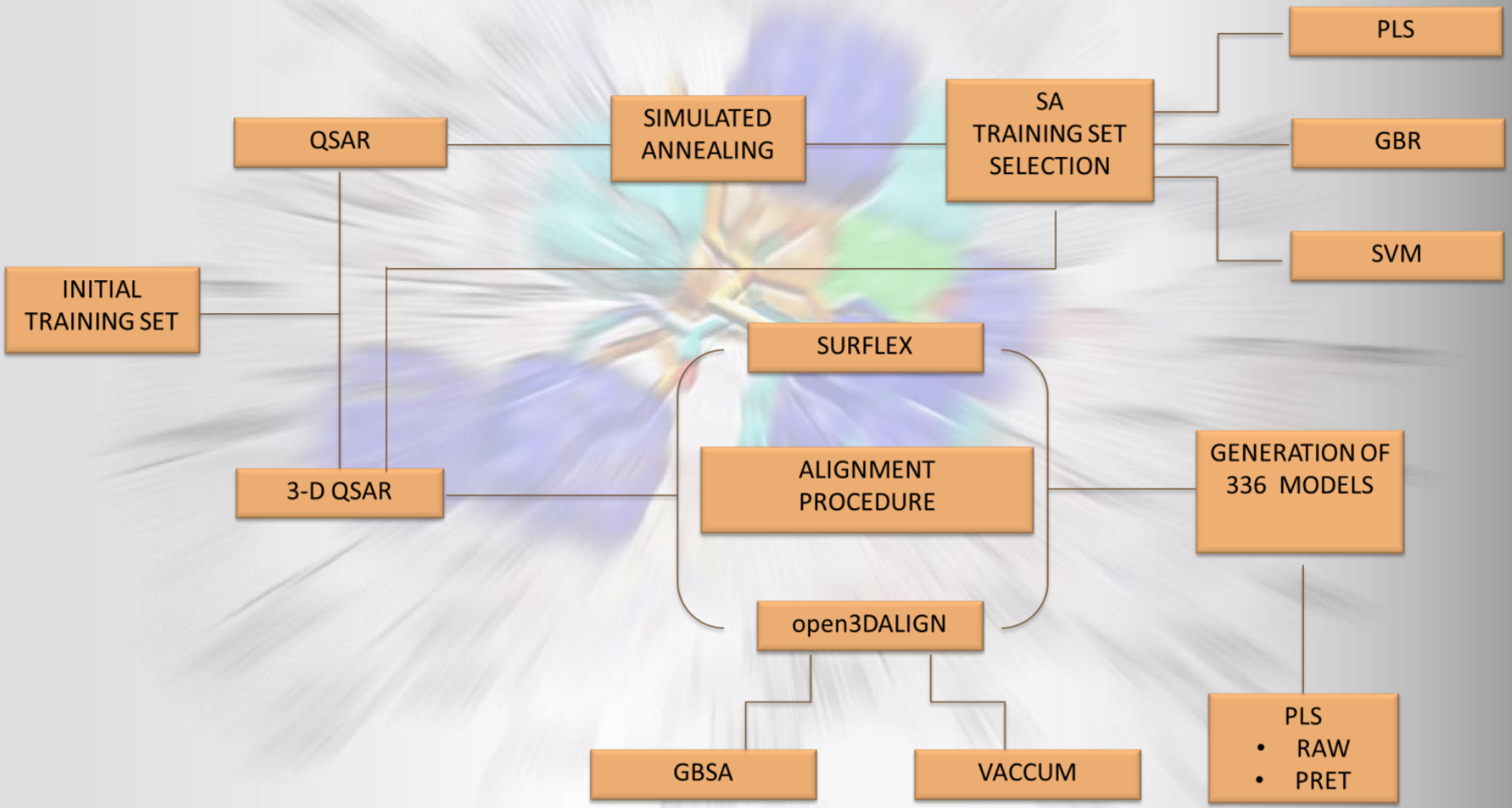

CANDIDA

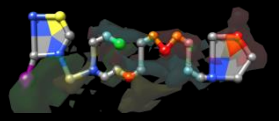

HSP90

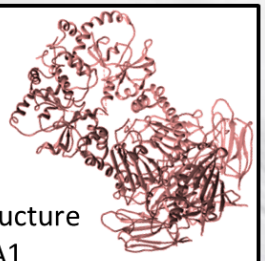

PDB CODE:
2CG9 Crystal structure of an HSP90-SBA1 closed chaperone complex

VGFR2

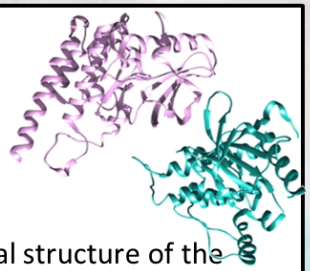

PDB CODE:
3DTW Crystal structure of the VEGFR2 kinase domain

ANTI CANDIDA DRUGS

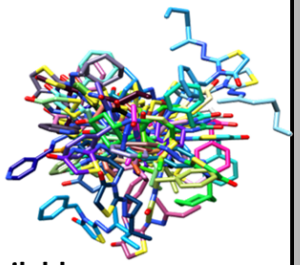

Target not available

Aliphatic chains (C_3-C_8)

Unsubstituted or alkyl-cycloaliphatic rings (C_5-C_8)

(Hetero)aryl or cycloaliphatic/bicyclic rings
= cyclopropane, furan, thiophene, cyclohexane, pyridine, (nitro-substituted)benzene, indole, benzofuran, benzodioxole, benzodioxane, chromene, naphthalene, phenantrene, ferrocene

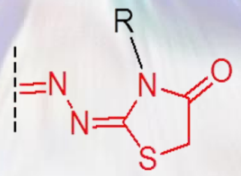

1,3-Thiazolidin-4-ones

SURFLEX

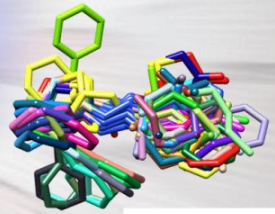

CHEMAXON

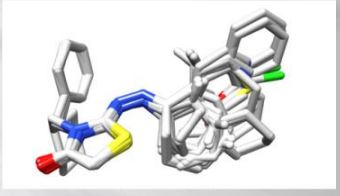

open3DALIGN

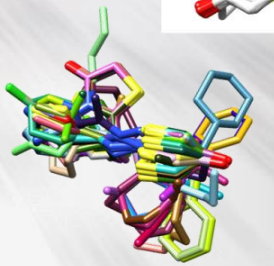

CANDIDA

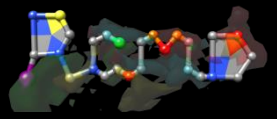

SUMMARY OF QSAR ANALYSIS RESULTS

INITIAL SET

RAW			SA VARIABLE SELECTION		
Estimator	**r^2**	**q^2 LOO**	**Estimator**	**r^2**	**q^2 LOO**
PLS	0.28	-0.15	PLS	0.28	0.20
GBR(huber loss function)	0.966	-0.48	GBR (huber loss fuction)	0.966	0.15
SVM (linear kernel)	0.30	-0.54	SVM (linear kernel)	0.27	0.044

FINAL SET

RAW			SA VARIABLE SELECTION		
Estimator	**r^2**	**q^2 LOO**	**Estimator**	**r^2**	**q^2 LOO**
PLS	0.59	0.37	PLS	0.61	0.52
GBR (lad loss function)	0.96	0.52	GBR (lad loss function)	0.95	0.79
SVM (linear kernel)	0.77	-0.57	SVM (linear kernel)	0.64	0.53

CANDIDA

SUMMARY OF 3-D QSAR ANALYSIS RESULTS

The final 3-D QSAR model was then selected on the basis of the statistical coefficients as follows: r^2, SDEC, q^2 and SDEP, and also on the lack of chance correlation as measured by a scrambling procedure.

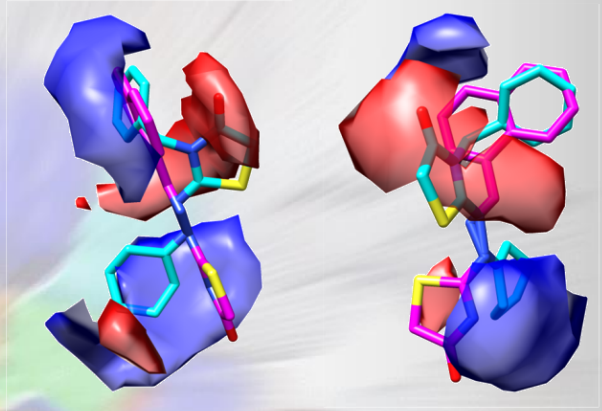

Probe	Referiment structure	Surflex-sim	open3Dalign/GBSA			open3Dalign/VACUUM		
			Atom	Pharm	Mixed	Atom	Pharm	Mixed
A	51A	0.261	0.208	0.456	0.235	0.237	0.422*	0.202
C	51A	0.264	0.210	0.468	0.241	0.226	0.389*	0.207
OA	51A	0.263	0.208	0.464	0.237	0.251	0.421*	0.190
N	51A	0.268	0.200	0.460	0.247	0.230	0.433*	0.214
NA	51A	0.254	0.209	0.472	0.241	0.240	0.435*	0.205
HD	51A	0.253	0.222	0.450	0.249	0.242	0.417*	0.205
e	51A	0.089	-0.003	-0.015	-0.019	-0.010	-0.021*	-0.001
d	51A	0.145	0.018	0.373	0.114	0.100	0.311*	0.013

q^2 values. K-fold cross validation

SIRT-2

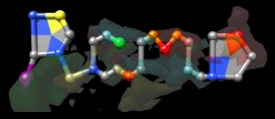

Cancer treatment and prevention by shifting necrosis into a RIP1-caspase 8-dependent apoptosis with a novel SirT inhibitor.

SIRT-2

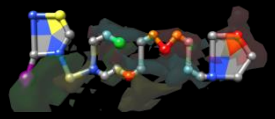

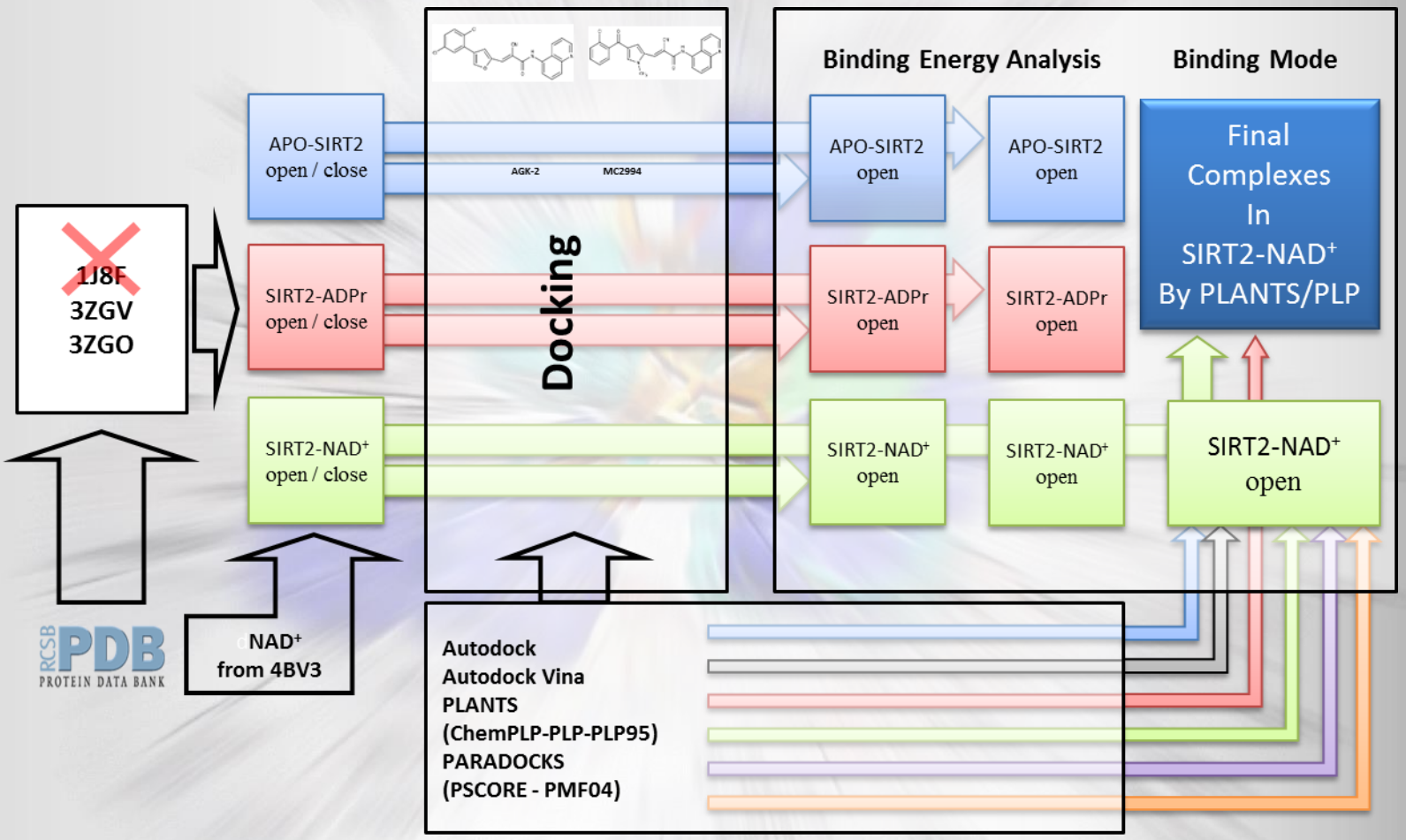

Antonello Mai. Sergio Valente. Sarah Meade. Maria Tardugno. Rino Ragno. Adele Pirolli. Angela Nebbioso. Vincenzo Carafa. Lucia Altucci and Aleksey Kazantsev. Submitted

SIRT-2

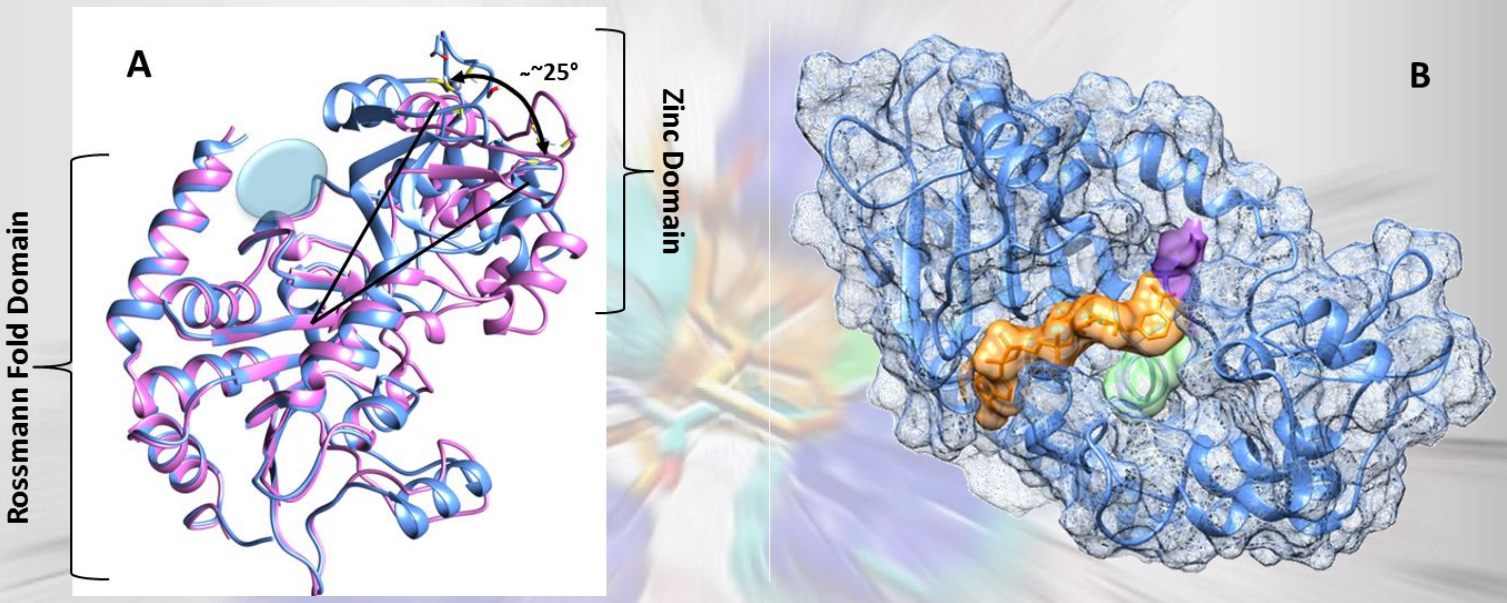

Figure 1. **A**: Superimposition of the open (pdb entry code: 3ZGO, $SIRT_{open}$, colored in magenta) and the closed (pdb entry code: c-3ZGV, $SIRT_{close}$, colored in cyan) SIRT2 conformations. The zinc domain shift is highlighted and the transparent blue ovale indicate the opened NAD+ binding site. **B**: SIRT2 (in cartoon) binding sites. The SIRT2 surface is shown in mesh, while the NAD^+ (orange), the acetyl lysine (violet) the leaving nicotinamide (green) binding sites are displayed in transparent solid surfaces

SIRT-2

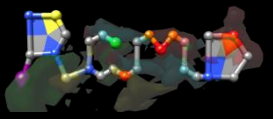

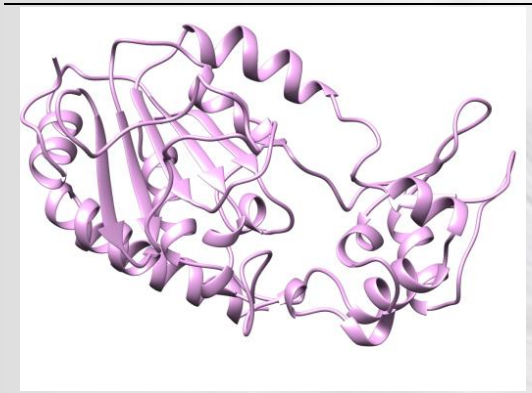

APO-SIRT2$_{close}$

SIRT2-ADPr$_{close}$

SIRT2-NAD$^{+}_{close}$

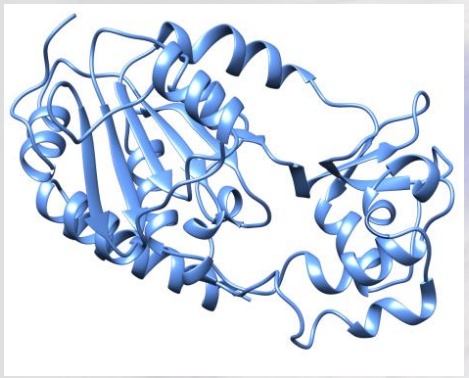

APO-SIRT2$_{open}$

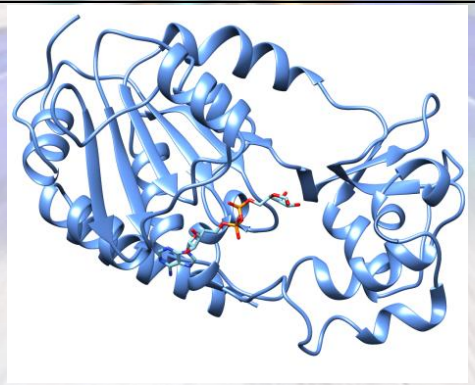

SIRT2-ADPr$_{open}$

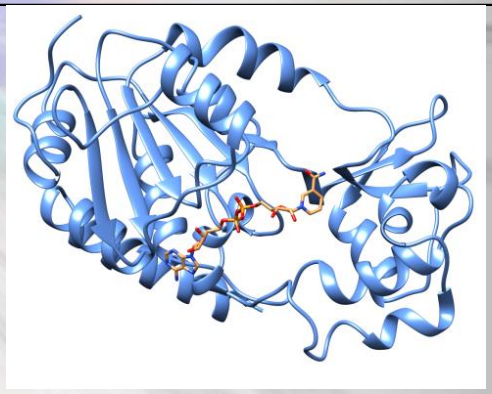

SIRT2-NAD$^{+}_{open}$

Crystal structures of the apo-enzymes and the binary complex with both NAD+ and ADPr The structures in Pink indicated the close form, while the blue structures the open form.

SIRT-2

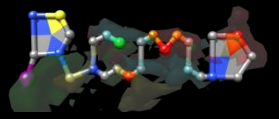

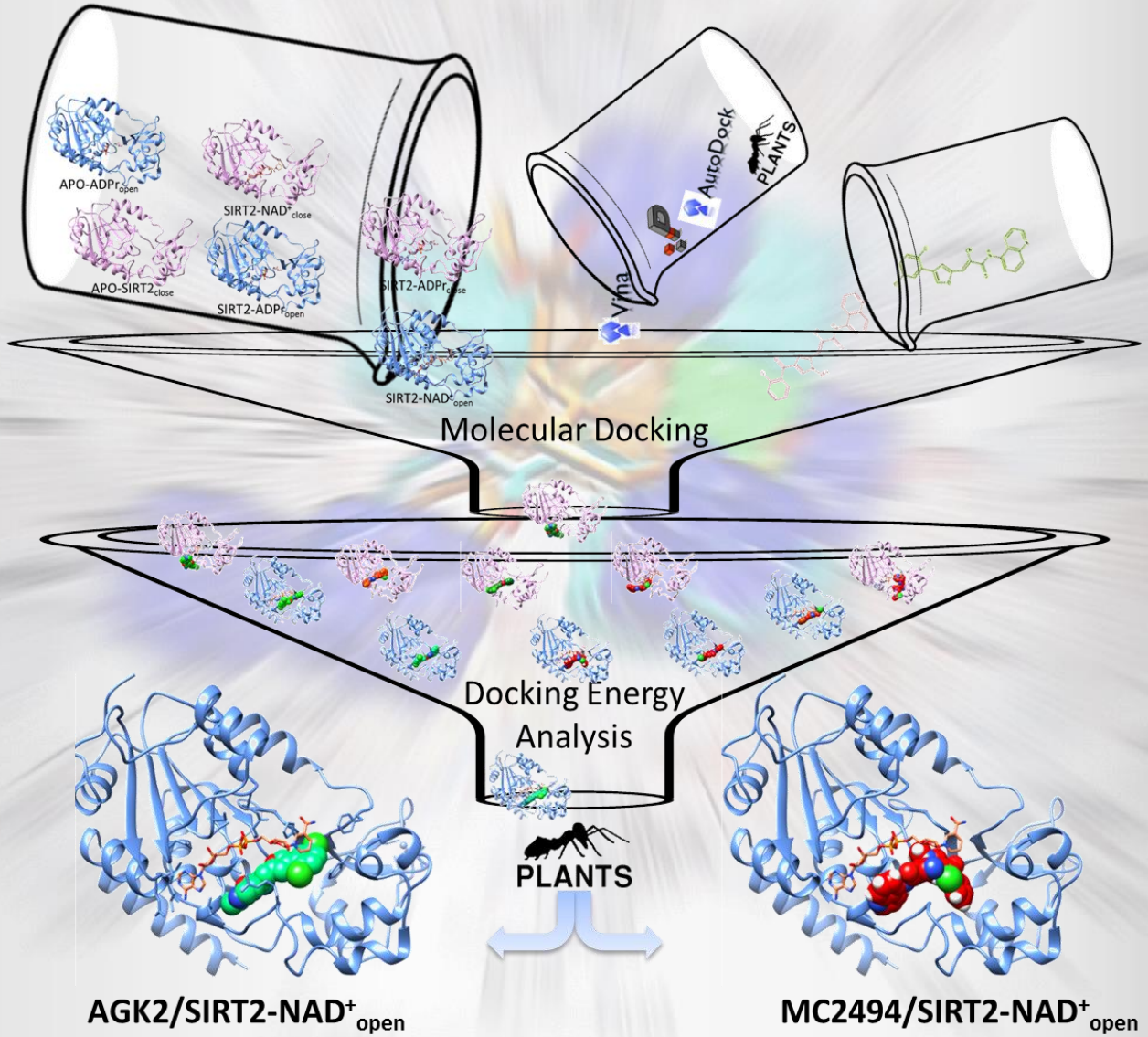
APO-ADPr$_{open}$
SIRT2-NAD$^+_{close}$
APO-SIRT2$_{close}$
SIRT2-ADPr$_{open}$
SIRT2-ADPr$_{close}$
SIRT2-NAD$^+_{open}$
Vina
AutoDock
PLANTS
Molecular Docking
Docking Energy Analysis
PLANTS
AGK2/SIRT2-NAD$^+_{open}$
MC2494/SIRT2-NAD$^+_{open}$

SIRT-2

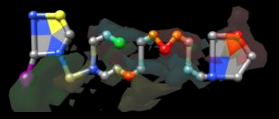

Docking scores for the lowest energy poses of AGK2 and MC2494 obtained from the different docking programs in the close SIRT2 conformations.

	AGK_2			MC2494		
Docking Program	APO-$SIRT2_{close}$	SIRT2-$ADPr_{close}$	SIRT2-NAD^{+}_{close}	APO-$SIRT2_{close}$	SIRT2-$ADPr_{close}$	SIRT2-NAD^{+}_{close}
AUTODOCK	-9.77	-9,68	-8,12	-9,86	-9,05	-9,02
VINA	-9.90	-9,00	-8,90	-8,80	-8,60	-8,50
PLANTS/CHEMPLP	-111.90	-84,55	-83,12	-113,01	-66,86	-71,83
PLANTS/PLP	-102.15	-77,83	-77,28	-107,75	-68,58	-68,07
PLANTS/PLP95	-166.31	-110,24	-117,44	-173,70	-108,07	-110,92
PARADOCKS/PSCORE	-875.36	-774,63	-559,87	-669,65	-683,24	-565,39
PARADOCKS/PMF04	-711.80	-507,38	-536,24	-664,84	-611,37	-566,16

Docking scores for the lowest energy poses of AGK2 and MC2494 obtained from the different docking programs in the open SIRT2 conformations

	AGK_2			MC2494		
Docking Program	APO-$SIRT2_{open}$	SIRT2-$ADPr_{open}$	SIRT2-NAD^{+}_{open}	APO-$SIRT2_{open}$	SIRT2-$ADPr_{open}$	SIRT2-NAD^{+}_{open}
AUTODOCK	-9.77	-10.89	-10.76	-9.86	-10.09	-10.60
VINA	-9.70	-9.90	-10.30	-9.80	-10.10	-10.90
PLANTS/CHEMPLP	-87.05	-99.12	-102.64	-87.88	-105.88	-102.55
PLANTS/PLP	-85.20	-95.48	-97.82	-87.05	-102.96	-105.41
PLANTS/PLP95	-134.44	-142.79	-141.65	-125.58	-149.53	-149.33
PARADOCKS/PSCORE	-582.25	-657.63	-680.78	-648.92	-720.78	-707.83
PARADOCKS/PMF04	-621.25	-605.51	-749.51	-717.78	-720.78	-813.65

SIRT-2

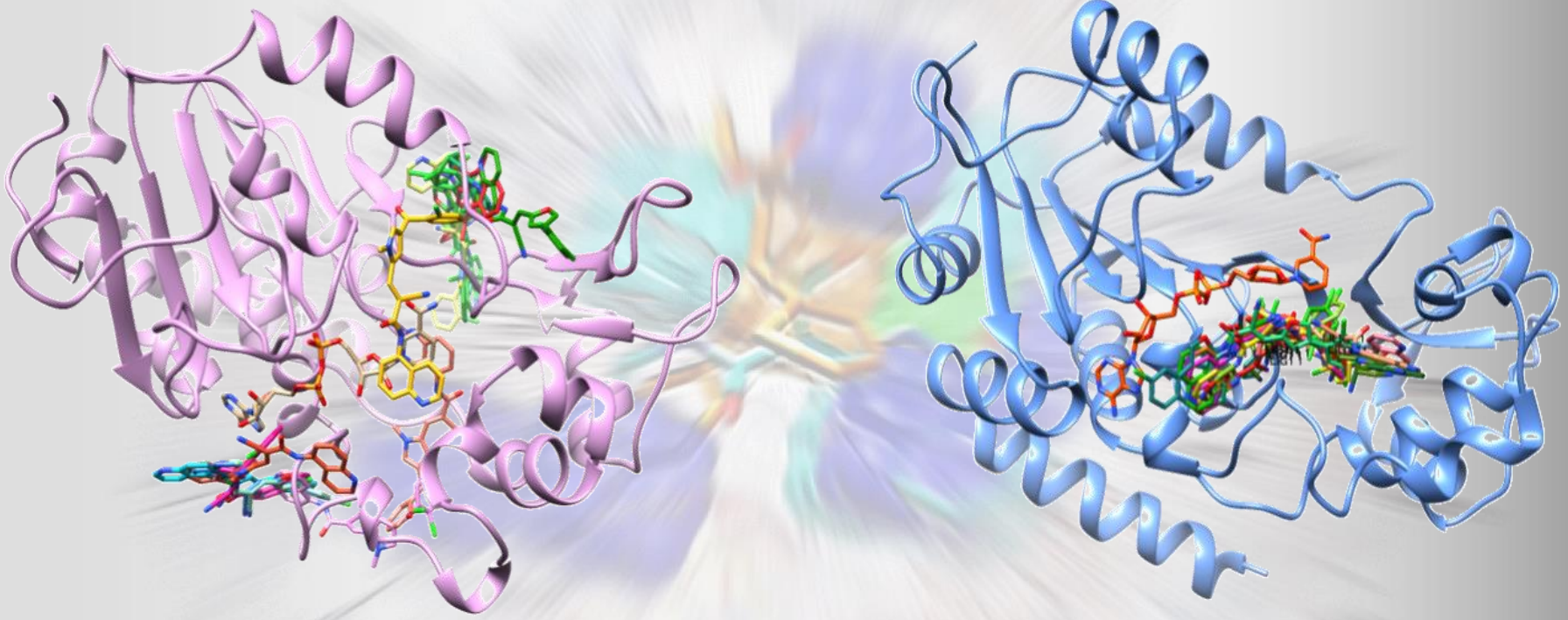

Examples of AGK2 and MC2494 docking poses. **A**: the disordered pattern in the APO-$SIRT2_{close}$. **B**: a convergence binding site in the SIRT2-NAD^{+}_{open}.

SIRT-2

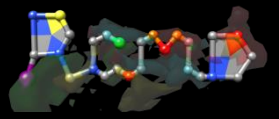

RMSD values calculated for the AGK2 and MC2494 poses. The values were calculated considering each program docking pose as the reference structure. In the last column are reported the average values.

Inhibitor	Docking Program Combination		AUTODOCK	VINA	PLANTS			PARADOCKS		Average
					CHEMPL	PLP	PLP95	PSCORE	PMF04	
AGK2	AUTODOCK		-	13.51	5.93	4.26	10.78	9.88	10.68	9.17
	VINA		13.51	-	13.35	13.55	14.63	5.52	4.36	10.82
	PLANTS	CHEMPL	5.93	13.35	-	3.59	9.55	10.51	11.16	9.01
		PLP	4.26	13.55	3.59	-	9.91	10.19	10.96	8.74
		PLP95	10.78	14.63	9.55	9.91	-	10.93	11.88	11.28
	PARADOCKS	PSCORE	9.88	5.52	10.51	10.19	10.93	-	2.22	8.21
		PMF04	10.68	4.36	11.16	10.96	11.88	2.22	-	8.54
MC2494	AUTODOCK		-	3.68	3.51	3.64	3.62	9.82	10.28	5.76
	VINA		3.68	-	1.30	1.54	1.56	9.82	9.72	4.60
	PLANTS	CHEMPL	3.51	1.30	-	0.45	0.47	9.89	9.81	4.24
		PLP	3.64	1.54	0.45	-	0.08	9.88	9.80	4.23
		PLP95	3.62	1.56	0.47	0.08	-	9.88	9.81	4.24
	PARADOCKS	PSCORE	9.82	9.82	9.89	9.88	9.88	-	3.54	8.81
		PMF04	10.28	9.72	9.81	9.80	9.81	3.54	-	8.82

SIRT-2

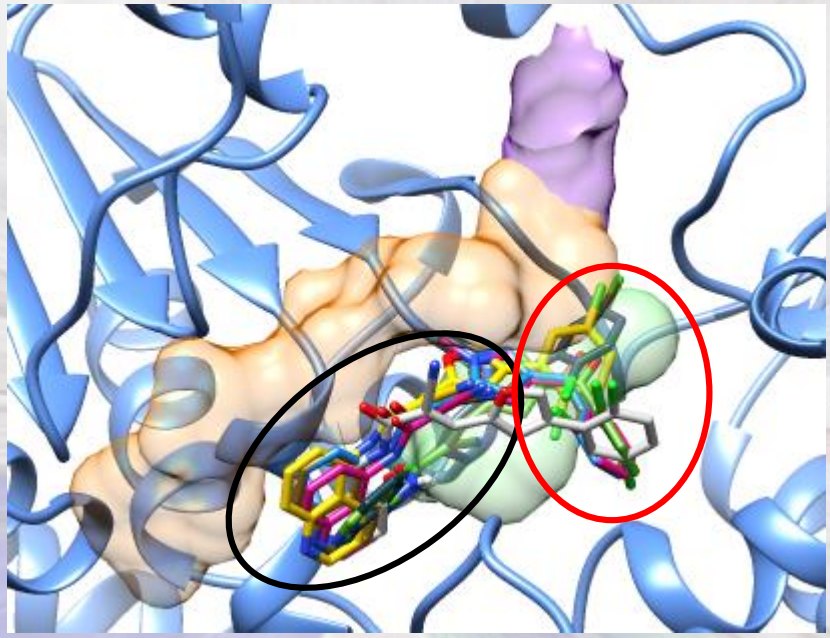

AGK2 and MC2494 AUTODOCK, VINA and PLANT overlapped poses. In the black circle are highlighted the quinolone and the five membered heterocycles. In the red circle the substituted benzenes. The NAD^+ (orange), acetyl lysine (violet) and nicotinamide (green) binding sites are displayed in transparent solid surfaces. The SIRT2 is in blue ribbon.

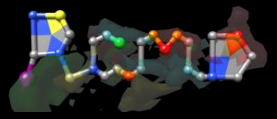

Binding of Azole Drugs to Heme. QSAR, Molecular Docking, Energy-Resolved Collision-Induced Dissociation and Car-Parrinello Molecular Dynamics Calculations

Alberto De Petris[§], Maria Elisa Crestoni[§], Adele Pirolli[¥], Carme Rovira[ǂ,ǂ], Javier Iglesias-Fernández[ǂ], Barbara Chiavarino[§], Rino Ragno[¥], and Simonetta Fornarini[§**]*

Binding of Azole Drugs to Heme

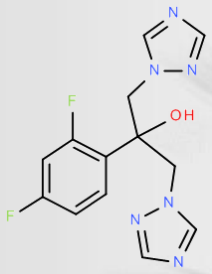

Fluconazole (**Flu**)

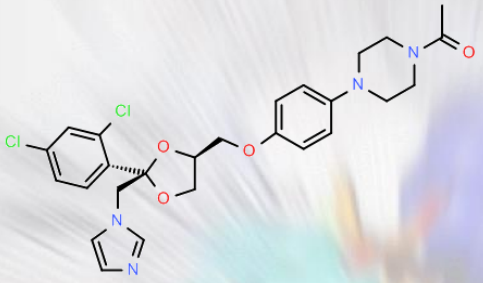

Ketoconazole (**Ket**)

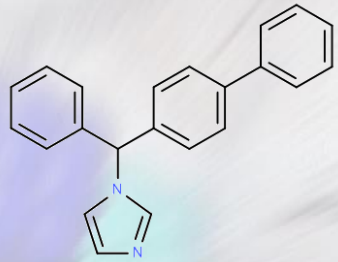

Bifonazole (**Bif**)

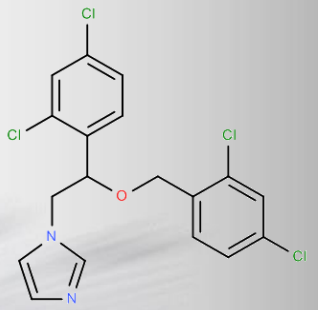

Miconazole (**Mic**)

Table 1. Comparison of IC_{50} Values for Candida albicans (caCYP51) and Human CYP51 (hsCYP51).

Drug	IC_{50} caCYP51*	IC_{50} hsCYP51*	Selectivity Index**
Bifonazole	0.30	0.80	2.7
Miconazole	0.072	0.057	0.8
Ketoconazole	0.064	0.43	6.7
Itraconazole	0.039	≈30	≈769
Fluconazole	0.051	>30	>588

*) Data are in μM (from ref 12).

**) Selectivity Index is the ratio between IC_{50}-hsCYP51 and IC_{50}-caCYP51

Binding of Azole Drugs to Heme

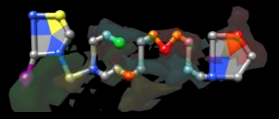

Table 3. Molecular descriptors used to derive the QSAR equation at 2 PLS principal components and the equation with the PLS coefficients.

ID	Flu	Ket	Itr	Mic	Bif
FeN	2.14	2.09	2.15	2.11	2.11
BDE	27.21	28.13	23.00	26.75	26.98
a_heavy_MW	294.18	503.22	667.34	402.02	292.26
$^{0}\chi^{v}$	11.34	21.49	28.87	16.03	13.29
$^{1}\chi^{v}$	6.39	12.64	17.16	9.00	8.09
$^{2}\chi^{v}$	4.84	9.80	13.15	7.15	5.81
$^{3}\chi^{v}$	3.21	7.06	9.70	4.85	4.27
$^{4}\chi^{v}$	2.25	4.60	6.24	2.42	3.08
PEOE_VSA1	5.11	28.58	24.01	9.30	4.57
PEOE_VSA12	0.00	11.69	5.79	0.00	0.00
PEOE_VSA2	0.00	4.79	0.00	0.00	0.00
PEOE_VSA6	6.07	29.27	36.19	58.54	84.93
SMR_VSA9	0.00	5.75	11.44	0.00	11.13
EState_VSA7	0.00	46.00	44.18	22.90	30.85
pIC_{50}	*7.29*	*7.19*	*7.41*	*7.14*	*6.52*

QSAR equation

pIC_{50} = (6,90959E-06***FeN**) +(-0.00031803***BDE**)+(0.000899826***a_heavy_MW**)+(4.95935E-05*$^{0}\chi^{v}$)+(5.23209E-05*$^{1}\chi^{v}$)+(4.55967E-06*$^{2}\chi^{v}$) + (1.92408E-05*$^{3}\chi^{v}$) + (8.32821E-05*$^{4}\chi^{v}$) + (-0.000810955* **PEOE_VSA1**) + (-0.000478093* **PEOE_VSA12**) + (-0.000357969* **PEOE_VSA2**) +(-0.004037796* **PEOE_VSA6**) +(0.000351406* **SMR_VSA9**)+ (-0.00232188***ESTATE_VSA7**) +6.96

Binding of Azole Drugs to Heme

Statistical parameters of the QSAR without and with the Carr-Parrinello derived parameters, namely Fe-N distance and BDE.

	q^2	r^2	Number of Variables
Without Fe-N distance and BDE	0.47	0.92	12
With Fe-N distance and BDE	0.50	0.92	14

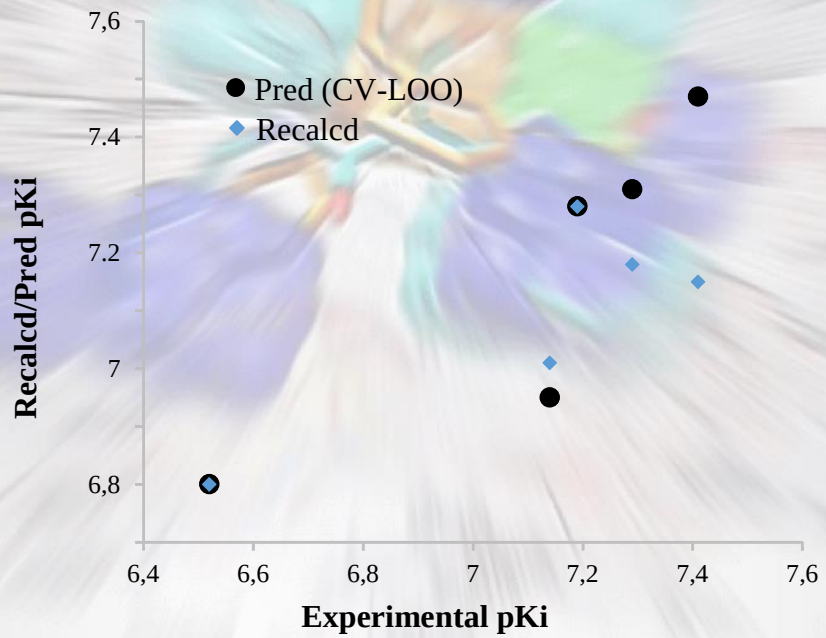

Experimental *vs* Recalculated/Predicted pIC_{50} values from QSAR model.

Binding of Azole Drugs to Heme

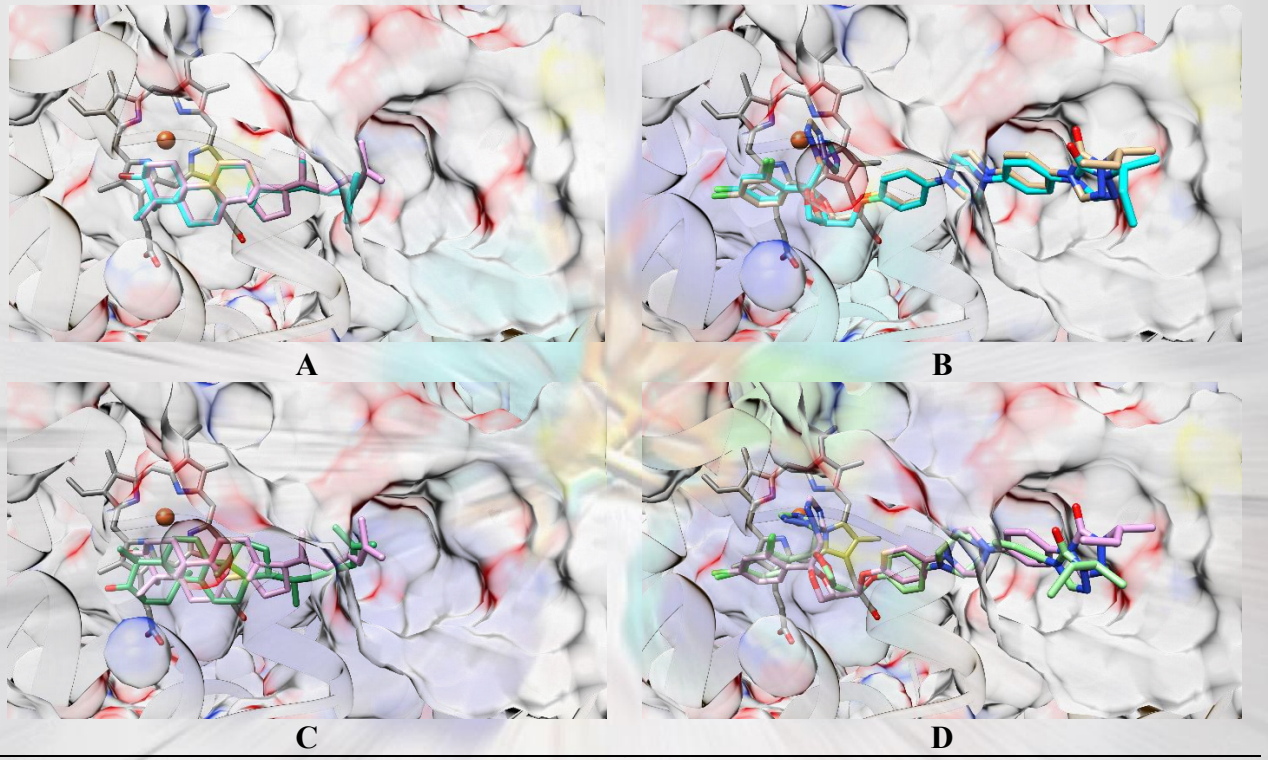

Re-docking and cross-docking by the Surflex program. A: re-docked lanosterol (cyan) ovelapped to the experimental conformation as found in 4LJX (pink); B: re-docked itraconazole (cyan) overlaped to the experimental conformation as found in 4KF0 (pink). C: cross-docked lanosterol (green) into 4K0F and compared to the experimental bound conformation (pink); D: cross-docked itraconazole (green) into 4LJX and compared to the experimental bound conformation (pink).

Binding of Azole Drugs to Heme

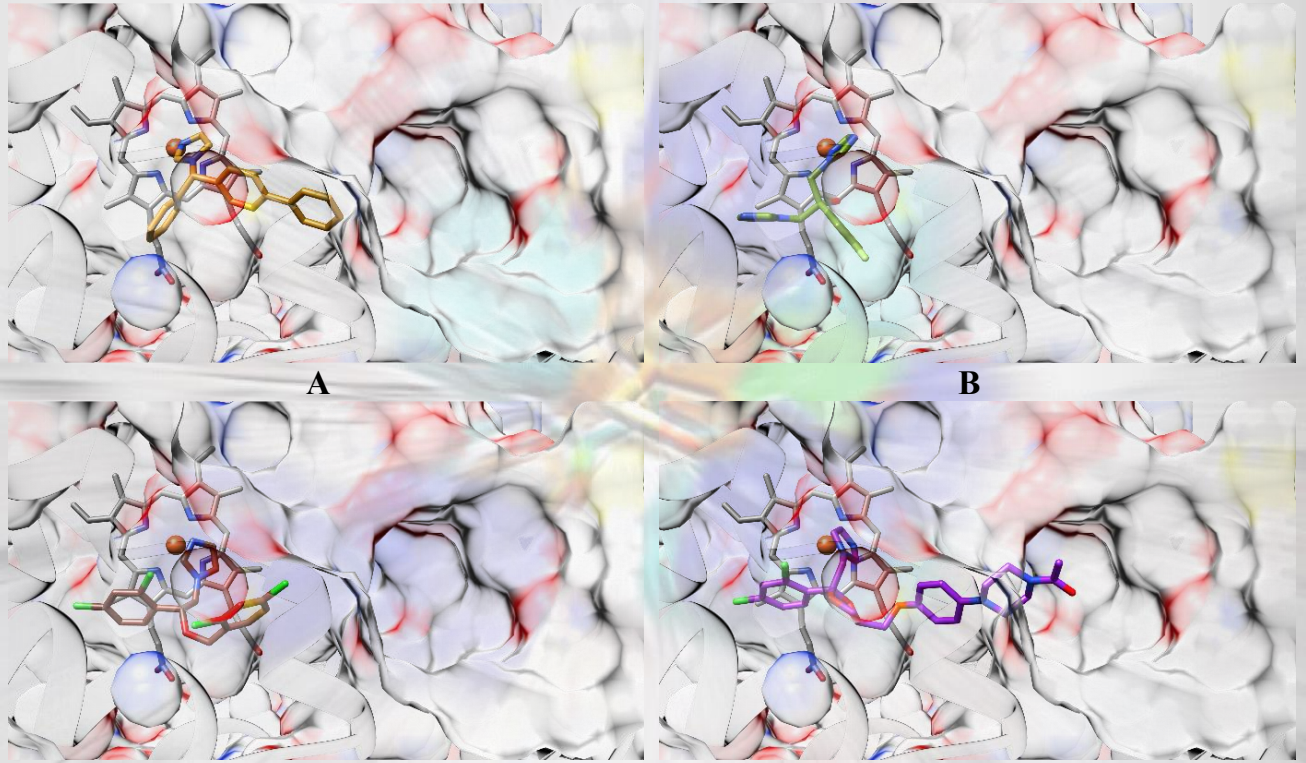

Binding mode of **Bif** (**A**), **Flu** (**B**), **Mic** (**C**) and **Ket** (**D**) as proposed by surflex-dock. For comparison purposes the orientation of the images is the same as those in Figure 6.

Binding of Azole Drugs to Heme

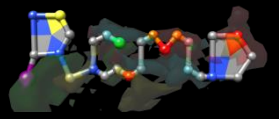

SVM kernel linear Kfcv 0.28

SBR **Kfcv** test set size 0.28% (5)

loss funct	*q2*	*r2*	*q2_raw*	*r2_raw*	*#features*
huber	*0,79*	*0,99*	*0,58*	*0,98*	*36*
loss funct	*q2*	*r2*	*q2_raw*	*r2_raw*	*#features*
ls	0,78	*0,99*	0,60	*0,99*	40
loss funct	*q2*	*r2*	*q2_raw*	*r2_raw*	*#features*
lad	0,79	*0,99*	0,60	*0,99*	38

0	***1***	***2***	***3***	***4***	***5***	***6***	***7***	***8***
(-)-spathulenol	*(z)-jasmone*	*2-caren-10-al*	*3-octanol*	*3-octanol acetate*	*alpha-cadinene*	*alpha-cadinol*	*alpha-cubebene*	*alpha-muurolene*
	0,0140952	0,0131414			0,0000000	0,2877270	0,0984807	0,0145990
0	***1***	***2***	***3***	***4***	***5***	***6***	***7***	***8***
(-)-spathulenol	*(z)-jasmone*	*2-caren-10-al*	*3-octanol*	*3-octanol acetate*	*alpha-cadinene*	*alpha-cadinol*	*alpha-cubebene*	*alpha-muurolene*
	0,000181	0,023175	0,025016	0,045353			0,073645	
0	***1***	***2***	***3***	***4***	***5***	***6***	***7***	***8***
(-)-spathulenol	*(z)-jasmone*	*2-caren-10-al*	*3-octanol*	*3-octanol acetate*	*alpha-cadinene*	*alpha-cadinol*	*alpha-cubebene*	*alpha-muurolene*
	0,000943	0,008594	0,045387	0,026676	0,001538	0,205244	0,017470	0,015068

Antimicrobial activity of essential oils against Pseudomonas syringae pathovar actinidiae 2 (PSA) agent of canker kiwifruit.

Elisabetta Vavala , Claudio Passariello, Federico Pepi , Marisa Colone , Stefania Garzoli , Rino Ragno , Adele Pirolli, Annarita Stringaro , Letizia Angiolella

PSA

Pseudomonas syringae pv actinidiae (PSA) is the causal agent of bacterial canker of kiwifruit. The canker of kiwifruit is a pandemic disease very difficult to treat. The prolonged treatment with cupric substances, still widely used for preventive treatments, has resulted in failure and resistance. Due to this resistance, alternatives to conventional antimicrobial therapy are needed. This study aims to analyse the phenotypic characteristics of this bacterium, search a new substance of natural origin able to contain the canker of kiwifruit and investigate its potential use when utilised in combination with other substances.

PSA

Microorganism and growth conditions. Two strains of Pseudomonas syryngae pv actinidiae (PSA) were obtained from a case of bacterial canker on A. chinensis in central Italy (Latina province) in 2011. Bacteria were isolated from trunk and from exudate and were identified by the techniques described below. The strains were cultured on nutrient agar (Oxoid) supplemented with 6 5% sucrose (NSA) and incubated at 25 27°C or room temperature for 24 h.

The results demonstrated that PSA was highly susceptible to synergic combination of sub-inhibitory concentration of Mentha suaveolens, Rosmarinus officinalis and TTO essential oils. This suggests that the combination treatments exerted a stronger bactericidal effect.

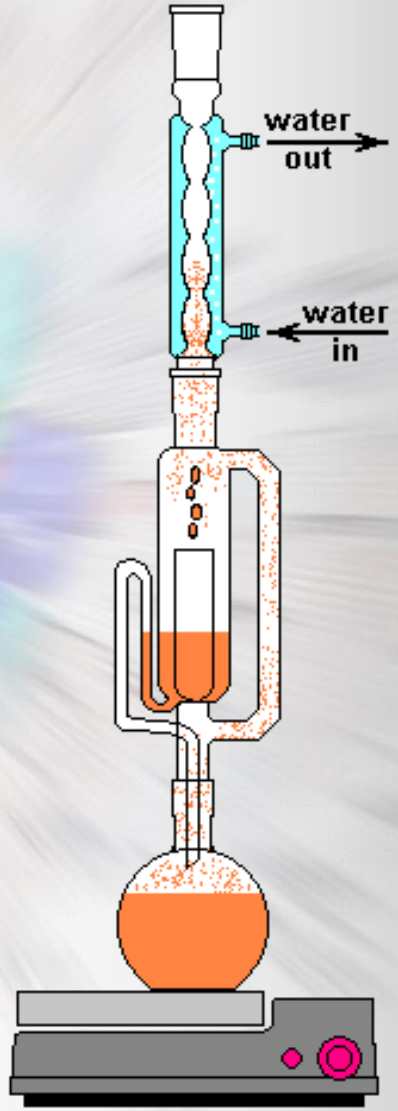

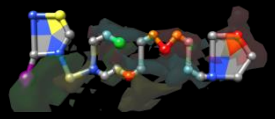

Combined 3-D QSAR Modeling and Molecular Docking Studies on Human Lysine-Specific Demethylase JMJD2A

JMJD2A

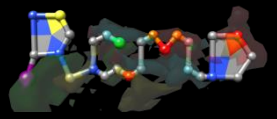

PDB

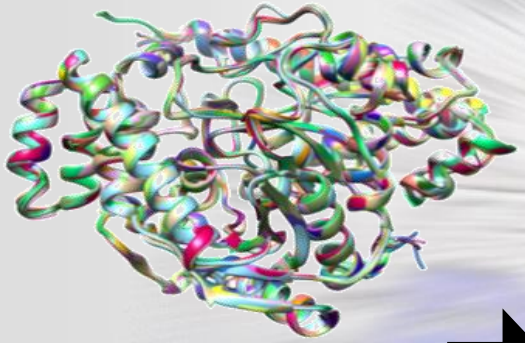

Docking Assessment

3-D QSAR

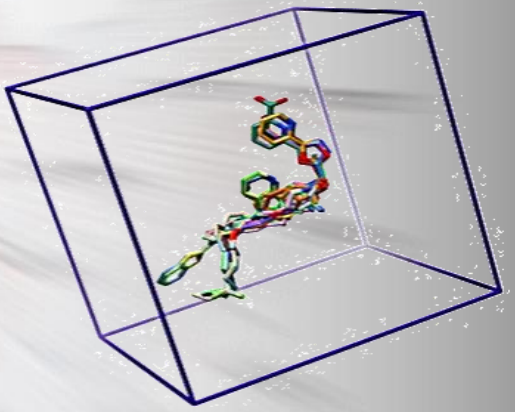

QSAR

SVM | GBR | RF

PLS | BR | KNN

JMJD2A

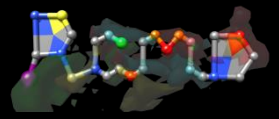

		DOCK	PARADOCKS pmf04	PARADOCKS pscore	PLANTS chemplp	PLANTS plp	PLANTS plp95	AUTODOCK	SURFLEX	VINA
ECRD	DA%	22,5	72,5	57,5	57,5	72,5	62,5	2,5	22,5	30
	sd	1,29	0,96	1,35	1,57	1,2	1,4	0,87	1,98	1,54
RCRD	DA%	30	40	25	60	60	65	2,5	32,5	22,5
	sd	1,44	1,27	1,64	1,24	1,17	1,08	0,7	1,4	1,38
ECCD	DA%	22,5	97,5	97,5	82,5	90	97,5	25	85	90
	sd	1,17	0,49	0,47	1,02	0,63	0,55	1,16	0,8	0,58
RCCD	DA%	62,5	85	75	77,5	92,5	90	17,5	85	62,5
	sd	1,02	0,68	1,01	1,1	0,62	0,55	1,08	0,72	0,9

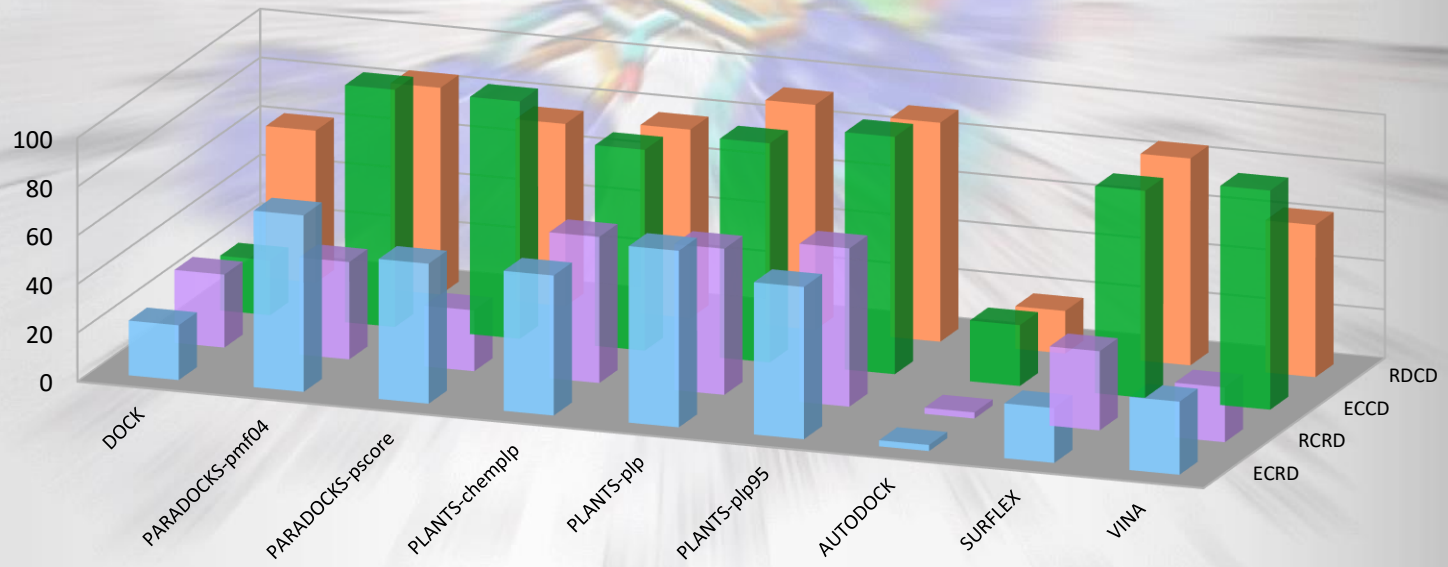

JMJD2A

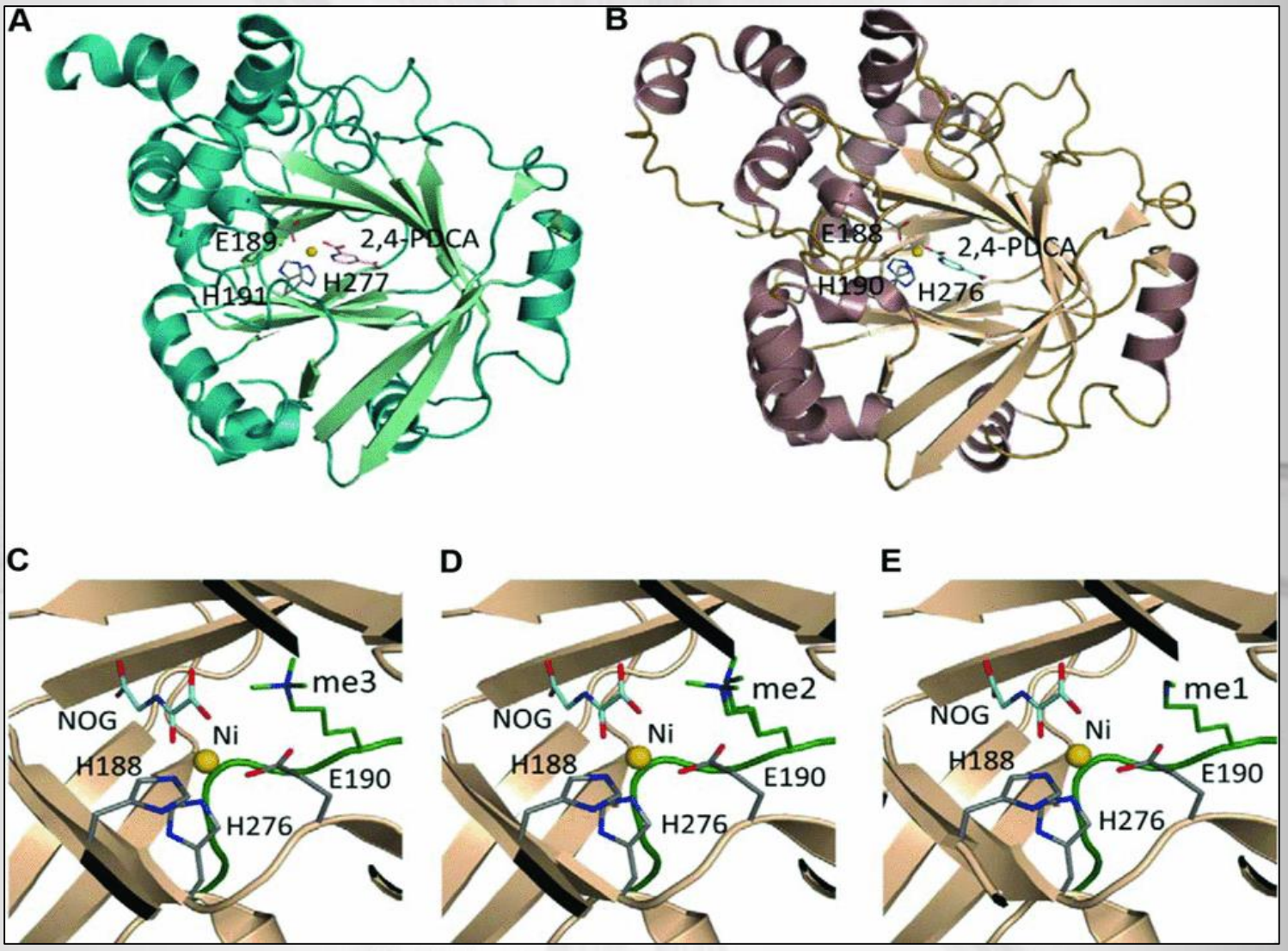
A
E189
2,4-PDCA
H191
H277
B
E188
2,4-PDCA
H190
H276
C
NOG
Ni
me3
H188
E190
H276
D
NOG
Ni
me2
H188
E190
H276
E
NOG
Ni
me1
H188
E190
H276

JMJD2A

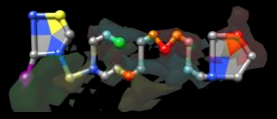

PLS Coefficients Plots
Red → positive
Blue → negative

Activity Contribution Plots
Greeen → positive
Yellow → negative

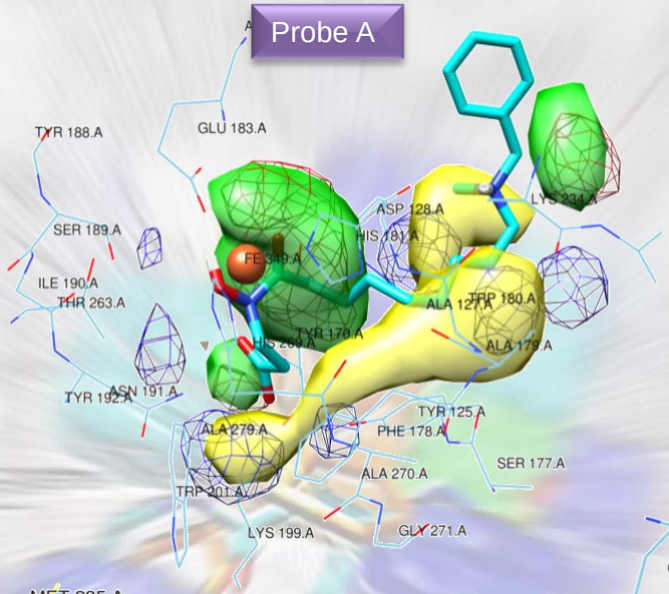

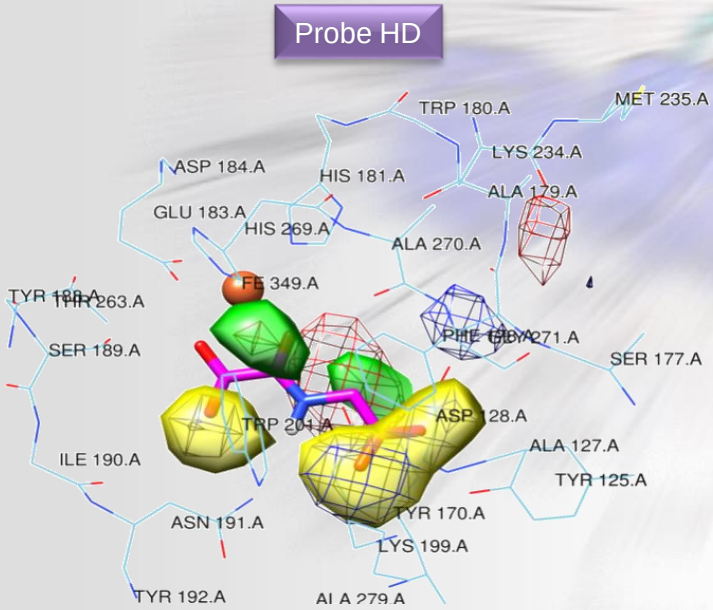

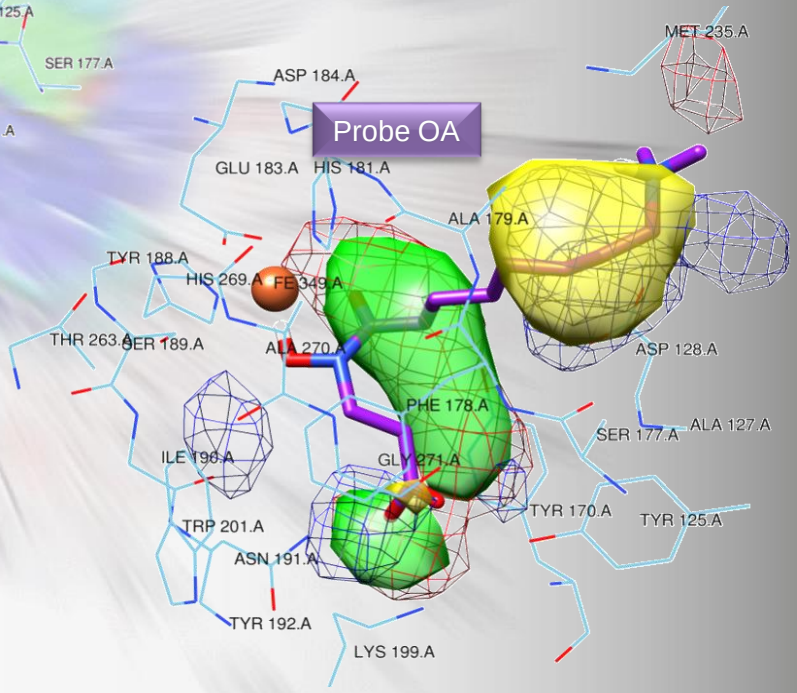

JMJD2A

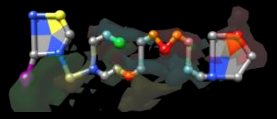

Training Set : **17 cmpds**

Activity Range (pMIC):
(2.74 Log unit,)

QSAR/SKLEARN LIBRARIES

CHEMBL

DATABASE	480,00
MW_SEL	479,00
LOGP_SEL	389,00
PSA_SEL	386,00

LOO

	r2	*q2*
PLSRegression_2	0,75	0,59
PLSRegression_3	0,89	0,65

Statistical/graphical Analyses

Prediction

^

	MIN	**MAX**	**MIN(+5%)**	**MAX(+5%)**
MW	284,39	608,05	270,17	638,45
LOGP	0,81	5,11	0,77	5,37
PSA	90,55	205,22	86,02	215,47

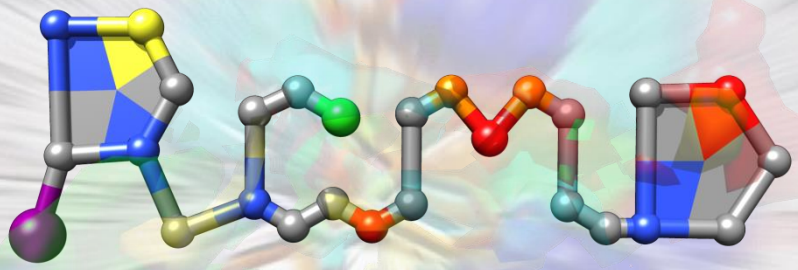

Thank you